July 2018

HYDROGEN EXCHANGE IDENTIFIES PROTEIN INTERFACES AND SIGNALING-RELATED CHANGES IN FUNCTIONAL CHEMORECEPTOR ARRAYS

Xuni Li

HYDROGEN EXCHANGE IDENTIFIES PROTEIN INTERFACES AND SIGNALING-RELATED CHANGES IN FUNCTIONAL CHEMORECEPTOR ARRAYS

A Dissertation Presented

by

XUNI LI

Submitted to the Graduate School of the
University of Massachusetts Amherst in partial fulfillment
of the requirements for the degree of

DOCTOR OF PHILOSOPHY

May 2018

Chemistry

HYDROGEN EXCHANGE IDENTIFIES PROTEIN INTERFACES AND SIGNALING-RELATED CHANGES IN FUNCTIONAL CHEMORECEPTOR ARRAYS

A Dissertation Presented

by

XUNI LI

Approved as to style and content by:

_____
Lynmarie K. Thompson, Chair

_____
Craig Martin, Member

_____
Igor Kaltashov, Member

_____
Peter Chien, Member

_____
Richard Vachet, Department Head
Department of Chemistry

DEDICATION

To my beloved parents, Xiaoling and Bailin – for their unselfish support and encouragement, and being my first teachers in my life.

To my husband, Yaohui – for his patience, friendship, sacrifice and endless love.

To my son, Sheldon – for letting me experience the kind of love that people freely die for.

To my golden retriever, Noodle – for his loyalty and loving me unconditionally.

ACKNOWLEDGMENTS

First and foremost, I would like to express my deepest appreciation to my advisor and mentor Dr. Lynmarie Thompson for her incredible patience and support. I am fortunate to be in her lab and be trained to a better scientist. Professor Thompson provides me continuous support and encouragement when I face obstacle. I am grateful for her guidance and support to show me how to think critically and be confidence in myself. Without her help, I will not be able to complete this project. She is the female role model in science that I can look up to.

I would like to thank my committee members: Dr. Craig Martin for his invaluable suggestions and recommendation of the project. Dr. Igor Kaltashov for providing useful information and aspects on the correlated and uncorrelated exchange in hydrogen exchange mass spectrometry. Dr. Peter Chien for providing insightful advices and suggestions of the project to complete this work. Previous committee, Dr. Robert Weis for developing the vesicle template assembly and characterizing the system enough to make this project possible, and you will be forever missed. Dr. Stephen Eyles for his mentoring, data interpretation and insightful discussion on the project. And special thank him for teaching me how to use different mass spectrometers and all the troubleshooting.

I would like to thank the past and present lab members in the Thompson lab, Dr. Daniel Fowler, Dr. Fe Sferdean, Shiela Jones, Dr. Michael Harris, Dr. Seena Koshy, Dr. Libbie Haglin, Maryam Kashefi and Aruni Karunanayake for all the discussions and useful

suggestions on the projects and troubleshooting in experiments. I am very thankful for the close friendship that I have with Seena Koshy and her continuous encouragement.

In addition, I would like to thank the past and present lab members on the 8th floor for helpful discussions and suggestions on projects, allowing me to use their instruments. Especially, Dr. Luis Ramirez-Tapia for teaching me how to do radioactive experiments, troubleshooting and resolve technical challenges in research. I would like to thank J.M. Stowe, Kay Fenlason, Carrie Penland for guiding me a long line of paperwork for completion of my Ph.D. A special thanks to the professional handyman, Bob Sabola, for repairing our broken instruments and modifying my icebox for the mass spectrometry experiments.

Furthermore, I would like to thank my amazing friends that I made during my graduate school. Especially, my close friend Hanwei Zhao for providing me useful suggestions and discussions on the hydrogen exchange mass spectrometry; Yuzhou Tang and Yichen Zhang for emotional support and encouragement.

Last but the least, my biggest thanks to my beloved family for their sacrifices that made my dream come true. My parents, Xiaoling and Bailin, have always supported me in everything. I need to thank my mom for her constant endless love to me and all the sacrifice she made for me. And last, I need to thank my husband, Yaohui, for his understanding, sacrifice, emotional support, faithful love and motivation.

I need to thank you from the bottom of my heart. This would not have been possible without each and every one of you.

"Many of life's failures are people who did not realize how close they were to success when they gave up."

-Thomas Edison

ABSTRACT
HYDROGEN EXCHANGE IDENTIFIES PROTEIN INTERFACES AND SIGNALING-RELATED CHANGES IN FUNCTIONAL CHEMORECEPTOR ARRAYS

MAY 2018

XUNI LI, B.A., UNIVERSITY OF MASSACHUSETTS AMHERST

B.S., UNIVERSITY OF MASSACHUSETTS AMHERST

Ph.D., UNIVERSITY OF MASSACHUSETTS AMHERST

Directed by: Professor Lynmarie K. Thompson

Chemotaxis is an ideal system for studying membrane protein signal transduction. Chemoreceptors are transmembrane proteins that sense chemicals in the environment and use this information to control a phosphorylation cascade that enables the cell to swim towards favorable environments. The receptors form a ternary complex with a histidine kinase, CheA, and an adaptor protein, CheW. These complexes assemble into membrane-bound hexagonal arrays that transmit the signal that controls CheA. It is widely accepted that ligand binding to the receptor causes a 2Å piston motion of a helix that extends through the periplasmic and transmembrane domains. But it is unclear how the signal then propagates through the cytoplasmic domain to inhibit CheA that is bound to the membrane-distal tip of the receptor, ~200Å away. Previous studies have suggested that signal propagation through the cytoplasmic domain involves inverse changes in the dynamics of the receptor.

In this study, we employ hydrogen deuterium exchange mass spectrometry (HDX-MS) to measure differences in structure and dynamics between defined states of the receptor. Functional complexes of a His-tagged cytoplasmic fragment (CF) are assembled on vesicles with CheA and CheW in three states for HDX-MS. Widespread correlated

exchange is observed, which indicates that the CF in functional complexes populates a long-lived unfolded state. Exchange is rapid throughout the CF except in the protein interaction region where CF binds CheA and CheW. These observations lead us to propose that signaling involves modulation of a folding equilibrium: binding of CheA (and possibly CheW) stabilizes the receptor, and CheA is bound in a kinase-on conformation. Thus, destabilization of the receptor will release this contact with CheA, which then adopts a kinase-off conformation. Both the kinase-off and demethylated samples of CF complexes exhibit faster HDX and less protection from exchange at long times at the binding interfaces with CheA. Thus we proposed that both the ligand-induced piston and demethylation destabilize the receptor, which releases its contact with CheA to turn off the kinase. Preliminary HDX results for CheA also set a stage for future analysis of the domain interactions of CheA in the functional complexes, and the differences that correlate with kinase activity. Ultimately, HDX-MS results will provide important information for deducing the signaling mechanism.

TABLE OF CONTENTS

Page

LIST OF TABLES

Table Page

LIST OF FIGURES

CHAPTER 1

INTRODUCTION

1.1. Overview of Bacterial Chemotaxis Receptor Function

Membrane proteins are involved in many the life processes, including cell division, antibiotic resistance and transmitting signals that allow bacteria to respond to the environment. Bacterial chemoreceptor complexes are an ideal system for understanding the mechanism of transmembrane signaling. Chemoreceptors are involved in sensing the chemical gradient in the environment and directing swimming towards favorable environments for survival.

Bacteria build remarkably large (~200 nm) multi-protein hexagonal arrays in their membranes to transmit signals that control their swimming direction (Briegel et al., 2009). These arrays enable this signaling system to respond with very high sensitivity and dynamic range (responds to concentrations ranging from nanomolar to millimolar) (Sourjik and Berg, 2002). These arrays are formed by chemotaxis receptors that are helical coiled-coil homodimers and cluster in patches at the cell poles. These chemoreceptors arrange themselves in the arrays to form trimer-of-dimers with a histidine kinase (CheA) and a coupling protein (CheW) (Briegel et al., 2008). The function of the ternary complex is to activate CheA. In the absence of ligand, the receptor will stimulate CheA to phosphorylate itself with ATP and then transfer the phosphate group to a regulator protein, CheY, or methylesterase, CheB. Phosphorylated CheY binds to the flagellar motor and causes the cell to tumble. Upon ligand binding, the receptor inhibits CheA which causes the cell to stop tumbling. Ligand binding also causes an increase in the rate of methylation of the receptor at specific Glu methylation sites in the cytoplasmic region, by a methyltransferase,

CheR. This increase of methyl groups on the receptor shifts it back to kinase-activating state (adaptation), which restores the basal tumbling level. Thus, the ligand-bound receptor is a kinase-off/ methylation-on state, and the ligand-free receptor is a kinase-on/ methylation-off state (Figure 1.1).

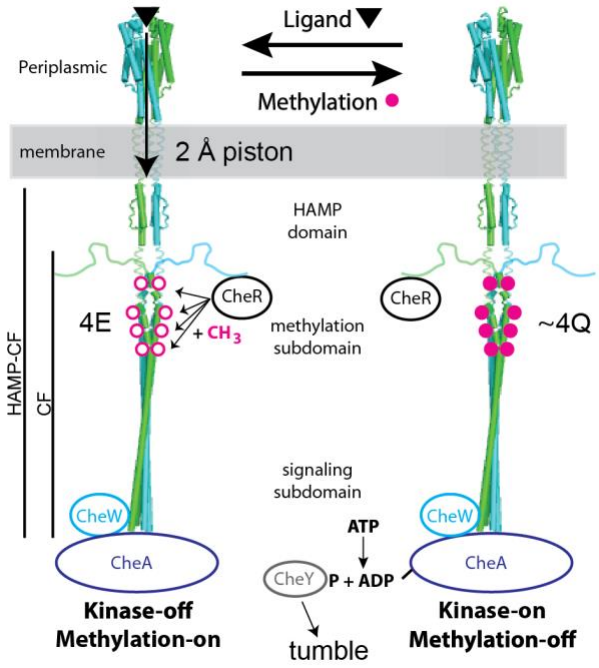

Figure 1.1. Schematic diagram of *E. coli* chemotaxis pathway and two receptor signaling states. The receptors are homodimers (green and cyan rods) that form ternary complexes with CheA (blue circle) and CheW (cyan circle). The methylation-on/ kinase-off state on the left occurs when ligand binds to the receptors which inhibits CheA phosphorylation. The methylation-off/ kinase-on state (right) promotes CheA phosphorylation and phosphotransfer to CheY (gray circle), which causes the cell to tumble. CheR (black circle) is the methyltransferase that methylates the receptors and shifts the equilibrium back to the kinase-on state.

1.2. Structure of Receptors and Functional Arrays

Bacterial chemoreceptors are 60 kDa α–helical homodimers that are 380Å long from the periplasmic tip to the cytoplasmic tip (Wadhams and Armitage, 2004). They contain a periplasmic domain, a transmembrane domain, and a cytoplasmic domain that couples with CheA and CheW. The cytoplasmic domain consists of a HAMP (histidine

kinases, adenylyl cyclases, methyl-accepting chemotaxis proteins, and phosphatases) (Aravind and Ponting, 1999) domain, methylation region, and protein interaction region that interacts with CheA and CheW (Kim et al., 1999) (Figure 1.1). Electron cryotomography (ETC) and fluorescence microscopy have shown these receptors organize themselves with CheA and CheW to form hexagonal arrays at the cell poles (Maddock and Shapiro, 1993; Zhang et al., 2007; Briegel et al., 2012; Cassidy et al., 2015). It is a challenge to investigate the mechanism within these functional complexes with native structure. Because transmembrane regions of membrane proteins are highly hydrophobic, which requires a detergent or lipid environment, it can be difficult to stabilize the structure and function. Detergent-solubilized receptors retain native ligand-binding affinity but are not methylated by CheR and do not activate CheA (Shrout et al., 2003). Intact receptors in vesicles and nanodisc preparations (Li and Weis, 2000; Falke and Hazelbauer, 2001; Amin and Hazelbauer, 2012) do exhibit methylation and kinase activity. However, samples in these preparations are heterogeneous due to impurities and lack of control of the orientation of the receptor. A recent electron cryotomography study shows that vesicle preparations produce heterogeneous orientations and structures of receptors, including formation of aggregates and zippers that are 9 nm center-to-center spacing (native hexagonal arrays are 12 nm) and both inward and outward oriented vesicles (Briegel et al., 2014). So far, there is no homogeneous preparation for functional complexes of intact receptors assembled with CheA and CheW. Weis and his coworkers (Shrout et al., 2003) have developed a method to assemble functional complexes of a cytoplasmic fragment (CF) onto the surface of large unilamellar vesicles (LUVs). The His-tagged CF binds the Ni^{2+} chelating headgroups of the vesicles as illustrated in Figure 1.2. Functional complexes assembled using this method

have been shown to form the same 12 nm hexagonal arrays as in native cells (Briegel et al., 2014), demonstrating that this a homogeneous sample with native structure and function.

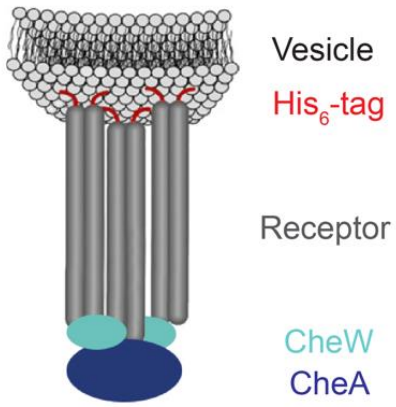

Figure 1.2. Vesicle template assembly of His-tagged CF with CheA and CheW. Templating vesicle contains lipids with nickel-chelating head groups that binds to the His-tag of the CF (dark gray) and assemble functional complexes with CheA (blue) and CheW (cyan) (Shrout et al., 2003).

1.3. Mechanism of Receptor Signaling and Proposed Role of Dynamics

The outstanding question in this field is how the signal propagates through the cytoplasmic domain. Cysteine cross-linking, solid state NMR and mutagenesis studies of intact receptors have shown that ligand binding induces a 2Å displacement of an alpha helix in the periplasmic and transmembrane domains of the receptor. (Chervitz and Falke, 1996; Ottemann et al., 1999; Falke and Hazelbauer, 2001). However, it is still unclear how the signal propagates through the cytoplasmic domain to control the activity of the kinase that is bound at the tip ~200Å away.

Changes in dynamics are proposed to propagate the signal through the cytoplasmic domain. Based on site-directed mutagenesis studies, Parkinson and coworkers proposed that the HAMP region is more dynamic in the kinase-on state and less dynamic in the

kinase-off state, and that the methylation region has the inverse dynamics (Zhou et al., 2009). Falke and coworkers used cysteine cross-linking to show that disulfide bonds formed in the methylation region lock receptors in the kinase-on state. Furthermore, mutations to Ala in the methylation region are locked in the kinase-off state but mutations to alanine in the protein interaction region are locked in the kinase-on state (Swain et al., 2009). Figure 1.3 illustrates the dynamic model that Parkinson, Falke and coworkers proposed based on these data: the HAMP and protein interaction regions are stabilized and the methylation region is destabilized in the kinase-off state relative to the kinase-on state. Studies thus far support proposed the decreased dynamics in the methylation region in the kinase-on or methylated state, but have also reported decreased dynamics in the protein interaction region. Electron paramagnetic resonance (EPR) and site-specific spin labels to measure the mobility of backbone of cytoplasmic domain of Tar in nanodiscs indicate that the methylation region is less dynamic in the kinase-on state, but ligand binding causes no changes in dynamics (Bartelli and Hazelbauer, 2016). Pulsed dipolar ESR spectroscopy was applied to kinase-on and kinase-off fusions of Tar with Aer HAMP domains. HAMP shows increased dynamics and the protein interaction region shows decreased dynamics in the kinase-on state (Samanta et al., 2015). A hydrogen exchange (HDX) study in functional complexes of CF, CheA, and CheW bound to vesicles shows both the methylation and protein interaction regions are less dynamic in the kinase-on state (Koshy et al., 2014). Finally, a recent INEPT (insensitive nuclei enhanced by polarization transfer) NMR study on similar functional CF complexes demonstrates that the N-terminal methylation helix shows more dynamics in the kinase-off state (Kashefi and Thompson, 2017).

A follow-up HDX study on the functional complexes is needed with more homogeneous samples. Greater vesicle surface area is needed to incorporate all CF to form hexagonal arrays with CheA and CheW. The prior study used different vesicle densities to control signaling state, but density could alter HDX via changes in solvent exposure. A locked-off mutant is used in this study to better control the signaling states. In addition, high resolution mass spectrometry with ion mobility separation (Waters Synapt G2Si) is used to obtain more overlapping peptides, contributing to both reproducibility and resolution.

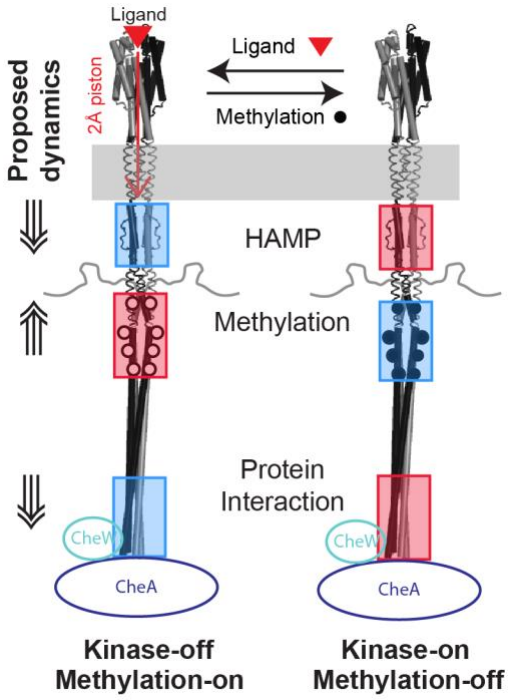

Figure 1.3. Overview of chemoreceptor with CheA and CheW and proposed dynamic model for signal propagation. Chemoreceptors (black and gray rods) are homodimeric, helical, and bound to CheA (blue circles) and CheW (cyan circles) in the protein interaction region. Proposed signaling mechanism starts with ligand binding (red triangle) causing a 2Å displacement of an α-helix toward the transmembrane region. The dynamic model proposes ligand binding inactivates CheA by reducing dynamics in the HAMP region (blue box), increasing dynamics in the methylation region (red box) and reducing dynamics in the protein interaction region (blue box) to form the kinase-off/ methylation-on state (left). The kinase-on/methylation-off state is proposed to have the inverse change in dynamics.

1.4. Hydrogen Deuterium Exchange Mass Spectrometry Studies of Structure and Dynamics

HDXMS is one of the methods that can monitor structure and dynamics of proteins in different states and conditions at both the global and local level. It can be used to understand the mechanism of protein folding pathways and binding interactions of protein. HDXMS has been used to monitor dynamics of membrane proteins in detergent micelles and nanodisc membranes (Chung et al., 2011; Morgan et al., 2011; Kacprzyk-Stokowiec et al., 2014; Duc et al., 2015).

HDX-MS can be conducted on native proteins using physiological conditions during labeling which will not disturb the structure of the proteins. Hydrogen deuterium exchange (HDX) is initiated by transferring proteins or complexes from protonated buffer to deuterated buffer. Hydrogens in proteins exchange continuously with deuterium in the solvent. Exposed or highly dynamic regions will exchange in a short time while the buried core of the protein and less dynamic regions will exchange much slower (Marcsisin and Engen, 2010), as illustrated in Figure 1.4.

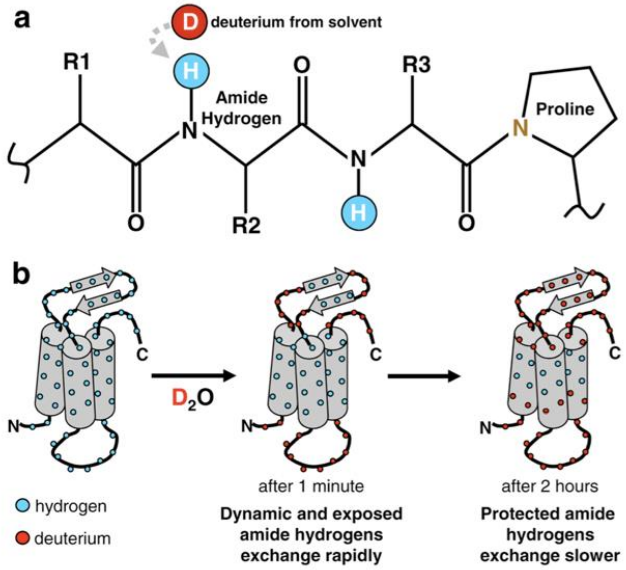

Figure 1.4. Overview of hydrogen deuterium exchange in proteins. (A) Amino acid sequence with backbone amide hydrogen (blue) and side chains (R1, R2, R3). After protein is placed in deuterated buffer, amide hydrogens exchange with deuterium (red) from solvent. (B) Amide hydrogens in solvent exposed regions (surface loops) and dynamic regions will undergo exchange in short time; amide hydrogens in protected and rigid region undergo exchange in long time (Marcsisin and Engen, 2010).

1.5. Objective of this study

Here, we report hydrogen deuterium exchange mass spectrometry studies of functional, native-like complexes in defined signaling states to gain insight into the signaling mechanism of chemoreceptors. We look at the effect of the methylation and signaling state on the CF in the functional complexes using vesicle template assembly with CheA and CheW. To investigate effects of methylation, HDX-MS is performed on vesicle-assembled native-like arrays prepared with CF4Q or CF4E, both assembled at the same density on vesicles. To prepare CF4Q in the kinase-off state, we introduce the A411V mutation, which has been shown to lock the receptor into the kinase-off state (Ames and Parkinson, 2006) and is also methylation-on (Kashefi and Thompson, 2017), so it faithfully mimics the signaling state and is not just a disruption of kinase activation. As discussed in the methods in Chapter 2, samples are optimized with sufficient vesicle surface area to incorporate all CF to form native-like hexagonal arrays with maximum CheA and CheW binding (Haglin, 2018).

Chapter 3 in this dissertation reports the HDX measurements on CF and provides insights into its properties and changes with methylation and signaling states. Within the functional complexes, all of CF shows evidence of populating a long-lived unfolded state (correlated HDX) and most undergoes rapid exchange, except the protein interaction region that is stabilized by interactions with CheA and CheW. The methylation and protein

interaction regions of the receptor CF are destabilized in the kinase-off state. Methylation stabilizes the entire CF, with similar but less dramatic changes between signaling states.

Chapter 4 describes preliminary HDX results on CheA. No significant differences between the kinase-on and kinase-off state are observed, perhaps because only 1/3 of CheA is in complexes. Some differences between free CheA and CheA in complexes suggest HDX will be informative when performed on samples with homogeneous CheA. This sets the stage for future studies to gain insights into the control of CheA kinase.

Finally, based on insights from HDX behavior of CF, Chapter 5 presents a new proposal that signal propagation involves an order/disorder transition of the cytoplasmic domain: protein binding at the tip stabilizes an ordered structure; piston and demethylation destabilize the structure and thus the interactions with CheA, leading to the kinase-off state. In summary, the work presented in this dissertation uses hydrogen deuterium exchange mass spectrometry to gain insight into the signaling mechanism in bacterial chemotaxis receptors, and the preliminary results on CheA demonstrate a promising approach for future studies to understand how the kinase activity is controlled.

CHAPTER 2

MATERIALS AND METHODS

2.1. Protein Expression and Purification

2.1.1. His-tag Tar cytoplasmic fragment (CF)

BL21(DE3) *E. coli* cells bearing plasmids for expression of His-tagged CF (pHTCF4Q, amp^R (Shrout et al., 2003) or pCF4Q.A411V, amp^R (Haglin et al., 2017)), and also co-transformed with pCF430 (tet^R), were streaked on Luria-Bertani (LB) agar platea with ampicillin (150 µg/mL) and tetracycline (10 µg/mL) and incubated at 37°C overnight. The following day, mutliple single colonies from the plate were each transferred to 2 mL LB broth containing the same concentration of antibiotics and grown until the optical density at 600nm (OD_{600}) reached 0.6 at 37°C with 200 rpm shaking. The 2 mL LB cultures were split into 3 culture tubes; one containing 100 µL culture was stored at 4°C for overnight growth later. The other two each contained 700 µL culture, and 1 mM IPTG was added to one of these to check protein expression; both were grown at 37°C with 200 rpm shaking for 1 hour. Gel samples of both cultures were prepared and run on 15% SDS-PAGE to check protein expression. Cells from the uninduced culture with the best expression were then inoculated into a 2 L culture containing the same concentrations of the antibiotics. This large scale culture was incubated in a 37°C shaker until OD_{600} reached ~0.6, followed by induction with 1mM IPTG overnight at 10°C. The cells was harvested by centrifugation at 3500 rpm (Beckman Coulter Allegra 6R Tabletop centrifuge, G38 swinging bucket rotor) at 4°C for 30 min, and then resuspended in lysis buffer (75 mM $K_xH_xPO_4$, 500 mM NaCl, 5 mM imidazole, and 1mM EDTA at pH 7.5) and lysed using microfluidizer (Microfluidics, Inc) at 16K psi on ice. 1mM PMSF was added every hour

to prevent proteolysis. Cell debris was separated using centrifugation at 10,000 rpm at 4°C for 90 min in a Sorvall RC-5B centrifuge, SS-34 rotor. Supernatant was then passed through a HisTrap FF Ni^{2+}-NTA affinity column (GE Healthcare) that had been equilibrated with 10 column volumes of equilibration buffer (75 mM $K_xH_xPO_4$, 500 mM NaCl, 5 mM imidazole at pH 7.5). The column was washed with 10 column volumes of wash buffer (75 mM $K_xH_xPO_4$, 500 mM NaCl, 50 mM imidazole at pH 7.5) to remove loosely bound proteins. CF was eluted with elution buffer (75 mM $K_xH_xPO_4$, 500 mM NaCl, 500 mM imidazole at pH 7.5) and located in the fractions by SDS-PAGE. Fractions containing CF were combined and treated with 5 mM EDTA to chelate any Ni^{2+} that came from the column. The CF solution was then placed in a dialysis bag with 7 kDa molecular weight cutoff, and dialyzed against dialysis buffer (75 mM $K_xH_xPO_4$, 75 mM KCl at pH 7.5) overnight at 4°C to remove EDTA and imidazole. Typically the dialysis was against 2L of dialysis buffer overnight, and then an additional 4 hour dialysis against 2L of fresh dialysis buffer, so that the calculated remaining EDTA and imidazole concentrations would be less than 0.01mM. The concentration of CF is determined using BCA assay (Thermo Scientific).

2.1.2. TEV-cleavable His-tagged CheA and CheY

His-tagged CheA (pTEV-cheA, kan^R) and CheY (pTEV-cheY, kan^R) (Kashefi and Thompson, 2017)were expressed in BL21(DE3) with 50 µg/mL kanamycin. Protein expression and growth protocols were the same as His-tagged CF except CheA was induced at 37°C for 3 hours, but CheY was induced overnight at 4°C. The same purification protocol was used to purify CheA and CheY, except using different buffers: lysis buffer (75 mM Tris-HCl, 100 mM KCl, and 1 mM EDTA at pH 7.4), equilibration buffer (75 mM

Tris-HCl, 100 mM KCl at pH 7.4), wash buffer (75 mM Tris-HCl, 100 mM KCl, 10 mM imidazole at pH 7.4), elution buffer (75 mM Tris-HCl, 100 mM KCl, 250 mM imidazole at pH 7.4), and dialysis buffer (75 mM Tris-HCl, 100 mM KCl at pH 7.4). Proteins were concentrated using 10 kDa cutoff Amicon filters centrifuged in a Beckman Coulter Allegra 6R Tabletop centrifuge, G38 swinging bucket rotor at 4°C at 3000 rpm until the volume was around 3 mL. A280 was used to estimate the concentrations of CheA and CheY (extinction coefficients of 25000 $M^{-1}cm^{-1}$ for CheA and 6970 $M^{-1}cm^{-1}$ for CheY (Lukat et al., 1991)) to choose conditions for TEV cleavage.

2.1.3. TEV-cleavable His-tagged CheW

DH5α bearing a plasmid for TEV-cleavable His-tagged CheW (pSJCW) was streaked on LB/Agar plate with 50 µg/mL amp^R and incubated at 37°C overnight. Note that pSJCW grew very slow and … The following day, a single colony from the plate was transferred to 2 mL LB broth which contained the same concentration of antibiotic and grown at 37°C with 200 rpm shaking until the optical density at 600nm (OD_{600}) reached 0.6. Expression check, large scale growth and protein purification were the same as described in previous section except that cell debris was spun down in a pre-chilled centrifuge (Sorvall, SS-34 rotor) at 10,000 rpm at 4°C for 1 hours followed by 1 hour of ultracentrifugation (Beckman Optima™ LE, 80K, SW28 rotor) at 28,000 rpm (104000 x g) at 4°C. Different buffers were also used: lysis buffer (50 mM $K_xH_xPO_4$, 300 mM KCl, 10 mM imidazole at pH 8.0); wash buffer (50 mM $K_xH_xPO_4$, 300 mM KCl, 50 mM imidazole at pH 8.0); elution buffer (50 mM $K_xH_xPO_4$, 300 mM KCl, 250 mM imidazole at pH 8.0) and verified by SDS-PAGE gel. Fractions contained proteins were combined and treated with 5 mM EDTA to chelate any Ni^{2+} came off from the column. Protein were

then placed in dialysis bag with 7 kDa molecular weight cutoff dialyzed in 2 L of dialysis buffer (75 mM $K_xH_xPO_4$ at pH 7.5) overnight at 4°C to remove EDTA and imidazole until EDTA and imidazole concentration is less than 0.01mM. Proteins were then placed in 10 kDa cutoff Amicon to centrifuge (Beckman Coulter Allegra 6R Tabletop centrifuge, G38 swinging bucket rotor) at 4°C at 3000 rpm until volume was around 3 mL. A280 was used to estimated concentration of CheW with coefficient 5120 $M^{-1}cm^{-1}$ before TEV cleavage (Gegner and Dahlquist, 1991).

2.1.4. TEV-protease

TEV-protease with an N-terminal His tag was expressed from the plasmid pRK793 (amp^R) given from D. Waugh, Addgene plasmid (Kapust et al., 2001) BL21(DE3)-RIL (cam^R) cells containing this plasmid were streaked on an LB/Agar plate containing 150 µg/mL ampicillin and 50 µg/mL chloramphenicol, and incubated at 37°C overnight. Liquid cultures were grown in LB containing the same antibiotic concentrations at 37°C until OD_{600} reached 0.6–0.8. Expression was then induced with 1 mM IPTG for 4 hours and TEV protease was purified as described in section 2.1.1. for purification of CF.

2.1.5. His-tag cleavage

After concentrating each protein to around 3mL, CheA, CheW and CheY were incubated with TEV-protease at 50:1 His-tagged protein: TEV-protease ratio. The mixture was stirred at 4°C for overnight and an additional 2 hours at 25°C. Cleavage by TEV was assessed by SDS-PAGE gel shift; if incomplete cleavage was observed, the sample was again incubated overnight at 4°C and assessed by SDS-PAGE. Cleaved proteins were then purified using the HisTrap column as described in section 2.1.1, except the TEV protease

was bound to the column and the flow-through contained the TEV-cleaved proteins. Proteins were then concentrated in 10 kDa molecular cutoff Amicon at centrifuge (Beckman Coulter Allegra 6R Tabletop centrifuge, G38 swinging bucket rotor) at 4°C at 3000 rpm until desired volume reached. BCA assay (Thermo Scientific) was used to determine the final concentrations of all CF, CheA, CheW and CheY solutions. Proteins were aliquoted into 1.5 mL Eppendorf tube, flash frozen with liquid nitrogen, and store at -80°C.

2.2. Lipid Vesicles

Vesicles were prepare using DOPC (1,2-dioleoyl-*sn*-glycero-3-phosphocholine) and the nickel-chelating lipid DOGS-NTA-Ni^{2+} (1,2-dioleoyl-*sn*-glycero-3-{[*N*-(5-amino-1-carboxypentyl)-iminodiacetic acid]succinyl}) (Avanti Polar Lipids) mixed in a 1.5:1 ratio. The mixture was dried under N_2 and kept under vacuum for at least 1 hour before resuspension in 1x kinase buffer (50 mM $K_xH_xPO_4$, 50 mM KCl, and 5 mM $MgCl_2$ at pH 7.5). The mixture was then subjected to five freeze thaw cycles: freeze with liquid nitrogen for 20-30 s, leave on the bench for 3 min, thaw in 37°C water bath for 3 min. Lipid vesicles were then extruded using an extrusion apparatus (Avanti Polar Lipids), for 15 passes through a 100 nm diameter pore size membrane. A total stock concentration of 3 mM lipid (DOPC and DOGS-NTA-Ni^{2+}) was used to assemble functional complexes; a final concentration of 725 µM lipid was used in the assembly. This lipid concentration was chosen to accommodate all of the 30µM CF in hexagonal arrays: (Appendix for detail). Concentrations of 12 µM CheA and 24 µM CheW were previously demonstrated to yield maximal kinase activity and native stoichiometries of ~ 6 CF:1 CheA: 2 CheW (Haglin, 2018). Note that another optimization study measured activity of CF4Q samples assembled

with lipid concentrations ranging from 1000-2500μM lipid: activity at 1300 μM lipid was ~ 20% higher than with 1000 μM lipid (25 μM CheA, 20μM CheW).

2.3. Vesicle and PEG Complex Assembly

Vesicle complexes were assembled with autoclaved water, phosphate kinase buffer, 1 mM PMSF in ethanol, 12 μM CheA, 24 μM CheW, 30 μM CF (CF4Q, CF4Q.A411V or CF4E), 725 μM vesicles (Shrout et al., 2003). PEG complexes were assembled with autoclaved water, phosphate kinase buffer, 1 mM PMSF in ethanol, 12 μM CheA, 20 μM CheW, 50 μM CF4Q, 7.5% w/v PEG 8000 (from 40% w/v stock), 4% w/v D-trehalose (from 40% w/v stock) (Fowler et al., 2010). Order of addition is the same as the order described. Complexes were incubated 4 hours or overnight at 37℃ water bath before testing the activity.

2.4. Biochemical Assays

2.4.1. Spectrophotometric kinase activity

CheA kinase activity was monitor by a UV spectrophotometric assay of the decrease of NADH over time in the absorbance at 340 nm for 90 seconds (Shrout et al., 2003). 2 μL of vesicles or PEG complex was mixed with 178 μL of CheY mixture which contained 55 μM CheY, 20 units of enzyme (lactate dehydrogenase (LDH) and pyruvate kinase (PK)) (Sigma-Aldrich) and phosphate kinase buffer; and 20 μL of fuel which contains 4 mM ATP, 2.2 mM phosphoenolpyruvate (PEP), and 250 μM NADH in phosphate kinase buffer at pH 7.4. The background of CheY was checked every time before checking any kinase activity of complexes. Adjusted kinase activity was calculated by subtracting the slope of the CheY-only background control from the slope of the

absorbance change at 340 nm of the complex. Specific kinase activity per CheA (s^{-1}) was calculated using (the adjusted slope as abs/min) x (1 min/60 sec) x (200 µL/2 µL) / (6220 abs/M (the molar absorptivity of NADH)) x (CheA concentration in M in the assembly). CheA concentration is either the amount of CheA bound to CF (determined by gel quantification in the protein binding assay, as described in 2.4.2.) for the specific activity, or the full 12 µM CheA for the total activity.

2.4.2. Protein binding assay

Sedimentation assay was used to determine amount of protein bound to vesicles to form functional complexes. 40 µL of functional complexes was spun in tabletop ultracentrifuge (Beckman TLX, TLA 120.2 rotor, 60,000 rpm, at 25°C for 30 min. Prior to sedimentation, a gel sample was prepared corresponding to the total amount of CF, CheA, and CheW in the sample. After sedimentation, the supernatant which contained unbound CF, CheA and CheW was removed and placed in a clean Eppendorf tube and used to prepare a supernatant gel sample. The pellet was resuspended to the original volume using 1x kinase buffer, vortexed, and used to prepare a pellet gel sample. Total, supernatant and pellet gel samples were run on 12.5 or 15 % acrylamide SDS-PAGE along with gel samples that contained known concentrations of CF, CheA and CheW for calibration purposes. Gels were then imaged by densitometry with a Gel Doc EZ Imager (Bio-Rad) and were analyzed with ImageJ software (Schneider et al., 2012). The amount of proteins bound were determined by $(I_{\text{Total}}\text{-}I_{\text{Supernatant}})$ x $[Protein]_{\text{Total}}$. The stoichiometry of the proteins in the arrays was calculated based on (1) the ratios of the concentrations calculated from the total minus super, and (2) the ratios of band intensities in the pellet fraction. The resulting stoichiometries from both methods were similar and were averaged to determine the

reported stoichiometry. Intensity of proteins in the known concentration gel samples (dilution series) were used to make a calibration curve to correct the background intensity and calculate the protein concentrations and ratios.

2.5. HDX Mass Spectrometry Measurements

2.5.1. HDX sample preparation

Vesicle-mediated complexes (CF4Q, CF4Q.A411V or CF4E with CheA and CheW) were assembled and incubated overnight as described in 2.3. Kinase activity and protein binding were checked (as described in 2.4) to be sure complexes were active and to monitor the amount of CheA and CheW bound to CF throughout the time-course of exchange. A desalting column was used for exchange (rather than dilution with a deuterated buffer) to avoid initiating dissociation of the complexes. Before initiating exchange, a 2 mL G10 Sephadex Zeba desalting column (Pierce Biotechnology) was pre-equilibrated with deuterated 1x kinase buffer (50 mM $K_xH_xPO_4$, 50 mM KCl, and 5 mM $MgCl_2$ at pD 7.5, pH reading 7.1 in D_2O) at 25°C as follows: spin at 2000 rpm for 2 min in a tabletop centrifuge (Beckman Coulter Allegra R Tabletop Centrifuge), discard the flow-through, add 1 mL deuterated buffer to the top of the column, spin again and repeat until the column has been exchanged with a total of 4 ml of deuterated buffer. Exchange was initiated by adding 1 mL of complexes to the pre-equilibrated column followed by centrifugation at 2000 rpm for 2 min at 25°C. The eluted solution of exchanged complexes was incubated in a 25°C water bath. For each time point of exchange, 22.5 µL was transferred into a pre-chilled Eppendorf tube containing 22.5 µL quench buffer (1% formic acid, 20% w/v glycerol, 1M GuHCl at pH 1.6) in a 0°C ice-water bath. Each sample was

immediately vortexed, flash-frozen in liquid nitrogen, and stored at -80°C. Undeuterated samples were prepared in the same manner, without the buffer exchange step on the column (22.5 µL of the initial assembly added to 22.5 µL of pre-chilled quench buffer and then flash-frozen).

The reversible heat denaturation of CF was used for preparation of a fully-exchanged sample (Murphy et al., 2001; Koshy et al., 2014), which was subjected to the mass spectrometry protocol to measure the back exchange for each peptide of our protocol. The fully-exchanged sample was prepared by applying 1 mL of a 30 µM CF4Q solution to a desalting column for buffer exchange into D_2O (as described above). The exchanged CF4Q was then placed in an 80°C water bath for denaturation for 1 hour, followed by 30 min in 0°C ice-water bath. The sample was prepared as described above (22.5 µL added to 22.5 µL of pre-chilled quench buffer and then flash-frozen).

2.5.2. HPLC column preparation and maintenance

For the MS analysis, a high performance liquid chromatography (HPLC) column was used for desalting and peptide separation. Before each set of mass spectrometry experiments, the HPLC column (2.1 mm x 5 cm C18 reverse phase column from Higgins Analytical) was connected to an LC pump (Agilent 1100G1312A) and cleaned by flowing 200 µL/min of Buffer B (0.1% formic acid in acetonitrile) overnight. At the end of each mass spectrometry experiment, the column was stored with 100% Buffer B. Every two months, the column was subject to deep cleaning by flushing with 20 column volumes of water, 20 column volumes of acetonitrile, 5 column volumes of isopropanol, 20 column volumes of heptane, 5 column volumes of isopropanol, and then 20 column volumes of acetonitrile at 200 µL/min.

2.5.3. HDX-MS data acquisition

2.5.3.1. HPLC method

The HPLC column (in a cold box, as described below) was equilibrated with 95 % Buffer A (0.1% formic acid in water). Peptides were eluted at 2 µL/min directly into the Waters Synapt G2Si with the following gradient programmed into the nanoACQUITY UPLC console system: 5% Buffer B for 3 min for removing salt in the sample, gradient from 5-50% Buffer B for 12 min to separate peptides, hold at 50% Buffer B for 3 min to elute all remaining peptides, 95% Buffer B for 7 min to clean the column, 5% Buffer B for 15 min to equilibrate the column for the next injection. Only the 3-18 min portion of this protocol was injected into the mass spectrometer. The initial 3 min (containing salts) and the 18-40 min cleaning (containing lipids) and equilibration were sent to waste.

2.5.3.2. MS method

At least one undeuterated sample was run on each day of MS experiments with collision ion-induced dissociation MS^E mode. The mass spectrometer was calibrated in positive ion mode using sodium formate. All samples were acquired in positive ion mode with ion mobility separation in mass range from 100-2000 Da. Lockspray of 556.2771 Da/e with single charge was continuously infused at 2 µL/min; the lockspray signal was acquired every 30 s for correcting mass.

2.5.3.3. MS protocol for minimizing back exchange and eliminating carryover

The HPLC separation was performed in an ice box filled with ice water to maintain the sample temperature near 0 °C, as shown in Figure 2.1. The metal connector (a) is connected to the HPLC output, and the orange and blue lines are waste. The PEEK

connector (b) is connected to the column, and the other end of the column is connected to the mass spectrometer sample injection port. During the experiment, the box is kept filled with ice to just above the metal clamp holding the injection valve (but below the top of the valve). This protocol was chosen to minimize back-exchange: the solvent is pre-chilled and sample travels through minimal length of tubing (59 cm before column and 69 cm after column) kept in ice water). Nano ACQUITY UPLC was connected to ice box bypassing the cold box from the Waters system and connect to HPLC reverse phase column and then directly connect to ion source on the Water Synapt. Valves and lines in ice box were cleaned using methanol, water, 50% isopropanol, 100% acetonitrile, each injected 5x with a 250 µL syringe in both load and inject positions. After connecting to the HPLC, the lines were further cleaned by loading 95% Buffer B for 15 min at flow rate 100 µL/min, with the valve first in the load position and then again with the valve in the inject position. The column was then connected to the PEEK connector (avoiding air bubbles) and then equilibrated with 95% buffer B for 15min at flow rate of 100µlL/min, then equilibrated with 95% buffer A for 15min at flow rate of 100µL/min. The ice is then added to the ice box.

Just before the MS experiment, samples were thawed for 1 min in a 0°C ice water bath, pepsin (Sigma Aldrich) was added in a 1:1 protein: enzyme molar ratio, digestion proceeded for 1 min at 0°C, and then x µL was immediately injected into the injection valve to flow through the column in icebox and into to mass spectrometer. One fully-exchanged control sample was run each day of experiments to measure back exchange.

After each sample acquisition finished, the end of the HPLC protocol (7 min 95% buffer B) removed lipid from the column, and the column was then equilibrated for 15 min

with 95% Buffer A to be ready for next sample. Blanks (water) run before each sample demonstrated that there was no carryover over from the previous sample. All exchanged samples were run in random order.

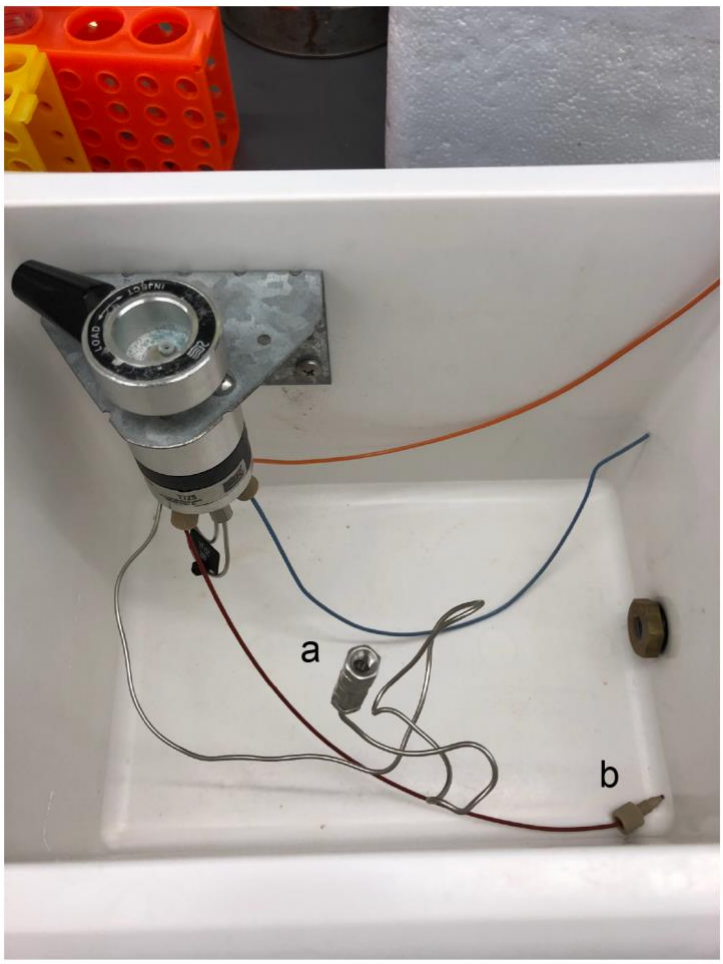

Figure 2.1. Icebox used to maintain minimum temperature during peptide separation step. Mass spectrometry sample was injected at the top of the valve. The metal connector (a) was connected to the output of the Waters HPLC and PEEK connector (b) was connected to the HPLC reverse phase column (not shown) for peptide separation. Both orange and blue lines are waste.

2.5.4. HDX data analysis

2.5.4.1. Peptides identification by ProteinLynx Global Service

Accurate mass and protein sequences were loaded on ProteinLynx Global Service (PLGS) version 3.0 software from Waters, to determine the peptides in the undeuterated samples. Process parameters were set to using 556.2771 Da/e as lock mass for charge 1, lock mass window as 0.25 Da with non-specific primary digest reagent. Peptide results generated by PLGS were then imported to DynamX version 3.0 software for further analysis.

2.5.4.2. Peptide analysis by DynamX

Peptide results were imported into DynamX version 3.0 with the minimum intensity set to 5000, minimum products per amino acid to 0.3, maximum sequence length of 25 amino acids, retention time RSD to 2%. Peptides were manually checked to be sure they each contained a minimum of 3 consecutive product ions. Mass spectra of different exchanged time point files were imported to DynamX for fetching ions and spectra. Each isotope peak in the isotopic distribution for a peptide was checked to be sure that all had the same retention time and ion mobility. Different charge states of the same peptide were checked to be sure they had the same retention time (but different mobilities). These were also compared across samples to be sure that the same peptide exhibited very similar retention times and mobilities in the different samples. The deuterium incorporation of each peptide was determined by subtracting the centroid mass of the undeuterated sample from that of the deuterated sample at each time point. The significant difference between two states is calculated using the standard error mean of all peptides that derive from the

standard deviation of the all peptides and multiply by the degree of freedom of 95% confidence interval. Note that standard error mean is calculated by the standard deviation of all peptides divided by the square root of number of data sets (Houde et al., 2011).

2.5.4.3. EX1 Analysis using HX-Express2

HX-Express2 (Guttman et al., 2013) was used to deconvolute bimodal patterns into two distributions. Analyzed mass spectra in ion mobility mode was copied and pasted into excel file in the format with m/z in the first column and intensity in the second column; time points were indicated in the first row. Note that this file format of m/z and intensity is needed in order for the program to run correctly. HX-express was installed as an Add-in for Excel (only works on a PC). Analysis was initiated with "Analyze Spectra" (HX-Express menu) followed by specifying the charge state (z), distribution width of 20% of BPI (base peak intensity), and using isotopic peak detection with peak tolerances of 5% of BPI (intensity) and 3 data points (m/z). The Output tab selections were Relative deuterium level, Plot width of isotopic distribution, and apply smoothing (4 channel Savitsky-Golay). Savitsky-Golay is only needed if smoothing has not been previously applied to spectra. Spectra were then analyzed using binomial fitting by providing the number of amides of the peptide and specifying a fitting asymmetry of 1. Note that number of amides of the peptide was calculated as the number of residues – 1– number of prolines. Each time point that exhibits a bimodal distribution was deconvoluted with "Double Binomial". Finally, "Summarize Double" provided a work sheet with the deconvolution plots and the probability and relative intensity of both low and high mass distributions.

CHAPTER 3

HDX-MS RESULTS ON FUNCTIONAL SIGNALING COMPLEXES: PROPERTIES AND SIGNALING-RELATED CHANGES OF THE RECEPTOR CYTOPLASMIC FRAGMENT

3.1. HDX-MS approach for investigating properties of receptor cytoplasmic domain within functional complexes

The use of hydrogen deuterium exchange mass spectrometry to investigate the structure and dynamics of the chemoreceptor cytoplasmic domain first requires preparation of homogeneous, functional complexes of the receptor with its cytoplasmic partners, CheA and CheW. Such homogeneity has not yet been achieved for the intact receptor, due to the challenge of controlling the orientation of insertion of the intact receptor into membrane vesicles or nanodiscs. Thus, we chose to assemble the receptor CF into native-like, functional complexes with CheA and CheW, using a vesicle templating method developed by Weis and coworkers (Shrout et al., 2003). CF in solution is not functional: it does not activate CheA and is not efficiently methylated. Binding of the His-tagged CF to the surface of large unilamellar vesicles containing a mixture of DOPC and DGS-Ni, in the presence of CheA and CheW, restores function (CF becomes a good substrate for methylation and also activates the CheA kinase) (Shrout et al., 2003) and also yields native-like hexagonal arrays (Briegel et al., 2014). Homogeneity is maximized by (1) using excess CheA and CheW to drive all of the CF into functional complexes, and (2) using a high enough lipid concentration to accommodate all of the CF in functional complexes, based on the known geometry of the hexagonal array observed in cells.

For HDX-MS experiments, these native-like complexes are assembled on vesicles and then tested for kinase activity and incorporation of proteins into the array (sedimentation assay). Measurements of kinase activity and protein binding, before hydrogen exchange and after exchange for 16 hours, demonstrate that complexes have high kinase activity, protein stoichiometries comparable to native arrays, and no significant loss of activity or proteins throughout the HDX time course (Figure 3.1 and Table 3.1). Table 3.1 shows that 47-68% activity and native-like protein stoichiometries are retained even at 48 hours. Thus, the properties observed by HDX-MS are those of the cytoplasmic domain of the receptor within functional signaling complexes. Complexes of the methylated-mimic CF4Q and the unmethylated CF4E (both kinase-on) are compared to reveal effects of methylation; complexes of the kinase-on CF4Q and the kinase-off CF4Q.A411V are compared to reveal effects of signaling state.

The HDX experiment is initiated by a rapid transfer of the complex from H_2O to D_2O. This is typically achieved in HDX studies by a 15-20-fold dilution into D_2O, but such dilution of a protein complex would cause dissociation during the exchange time course. Therefore, exchange is initiated using a spin column, pre-equilibrated with deuterated kinase buffer at 25 ˚C. For each exchange time point, an aliquot is removed, added to pre-chilled quench buffer, and immediately flash-frozen. For MS analysis, each sample of the hydrogen exchange series is thawed and digested with pepsin at 0˚C, followed by LC-ESI-MS analysis on a Waters Synapt G2Si Q-TOF mass spectrometer. At least one undeuterated sample and one fully deuterated sample (prepared by reversible heat denaturation of CF in deuterated buffer) are included as controls on each day of mass

spectrometry; the fully deuterated sample (which undergoes back exchange equivalent to that of all of the samples) provides a measure of complete exchange.

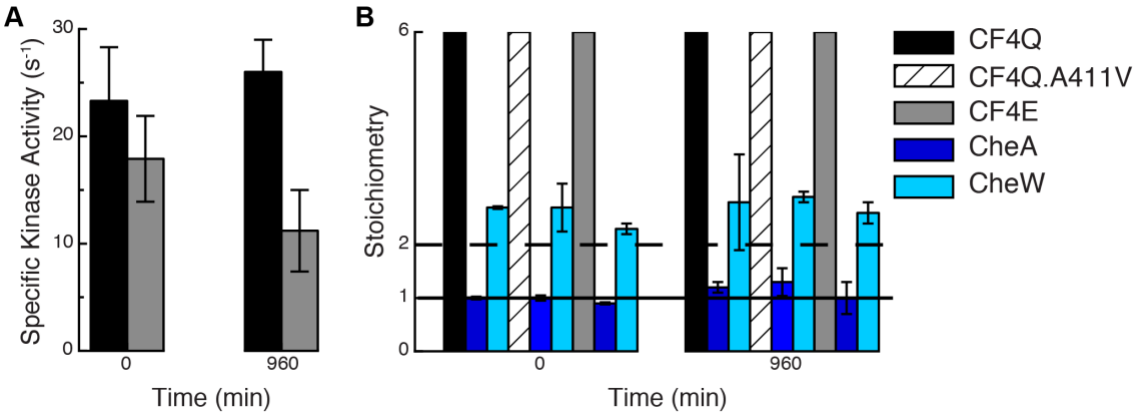

Figure 3.1. Kinase activity and protein binding within complexes of CF remain constant over the timecourse of deuterium labeling. (A) Specific activity of CheA kinase assembled into native-like complexes with CheW and His-tagged CF4Q (black) or CF4E (gray) bound to vesicles. For each complex, kinase activity is high and does not change significantly between 0 and 960 min (=16 hr). Activities are averages of four replicates measured on two different days; error bars indicate ± one standard deviation. (B) Protein stoichiometries, determined as the ratio of proteins in the sedimented complexes (SDS-PAGE band intensities), within complexes of CF4Q and CF4E (both kinase-on) and CF4Q.A411V (kinase-off). Sedimented CF (24-29 μM) was set to 6 for calculations of the ratio of CF to CheA (blue) and CheW (cyan). Horizontal lines correspond to the levels of CheA (solid line) and CheW (dashed line) observed in native arrays.

Table 3.1. Kinase activity and protein incorporation into functional complexes of CF4Q, CF4Q.A411V, and CF4E, assembled on vesicles with CheA and CheW.

Time	Specific Activity[a] (s^{-1})	CF[b] (μM)	CheA[b] (μM)	CheW[b] (μM)	CF:CheA:CheW[c]
CF4Q					
0min	23.3 ±5	24.3 ±2	3.7 ±0.1	10.8 ±0.1	6: 1: 2.7
960min (16 hr)	26 ±3	27 ±1.3	4.75 ±0.4	13.2 ±3.7	6: 1.2: 2.8
2880 min (48 hr)	15.8 ±3.2	25 ±0.6	4.6 ±0.1	12 ±1.3	6: 1.2: 2.8
CF4Q.A411V					
0min	0.04 ±0.14	24.4 ±0.5	3.75 ±0.2	11.6 ± 1.8	6:1:2.7
960min (16 hr)	0.01 ±0.11	28.4 ±5.2	4.85 ±1.2	13.5 ±0.7	6:1.3:2.9

2880 min (48 hr)	NA	26.2 ±2.6	4.35 ±1.1	11.9 ±1.9	6:1.5: 2.9
CF4E					
0min	17.9 ±4	26.3 ±7.3	3.4 ±0.1	9.6 ±0.4	6:0.9:2.3
960min (16 hr)	11.2 ±3.8	29.3 ±3	5.3 ±1.6	12.6 ±1	6:1:2.6
2880 min (48 hr)	8.4 ±1	29 ±3.4	6.4 ±1.2	15.1 ±1.1	6:1.3:3

[a]Activities are average of four replicates (measured on two samples on two different days); error bars indicate ± one standard deviation.
[b]Protein concentrations in the sedimented complexes, based on SDS-PAGE band intensities.
[c]Stoichiometry of proteins in the sedimented complex was calculated by setting the CF concentration (24-29 μM) to 6 to calculate the ratio of CF to CheA and CheW.

The peptides shown in Figure 3.2 were identified in the mass spectra of the undeuterated (0 min time point) samples, acquired in collision-induced dissociation mode for peptide sequencing. The Waters Synapt G2Si instrument software, ProteinLynx Global Server (PLGS) and DynamX version 3.0 were used to identify peptides with minimum MS signal intensity of 5000, maximum sequence length of 25, and minimum products per amino acid of 0.3, resulting in a total of 86 CF peptides, 183 CheA peptides, and 52 CheW peptides (averages for the different samples). This protocol yielded an average CF peptide coverage of 80-88% and amino acid redundancy of 2.6-3.4 for the functional complexes of CF4Q, CF4Q.A411V and CF4E. The peptides of the completely exchanged CF4Q control sample exhibited 11-43% back exchange for our protocol (average 25%), with little variation (1%) for experiments performed on different days.

A. CF4Q Peptide Coverage

B. CF4Q.A411V Peptide Coverage

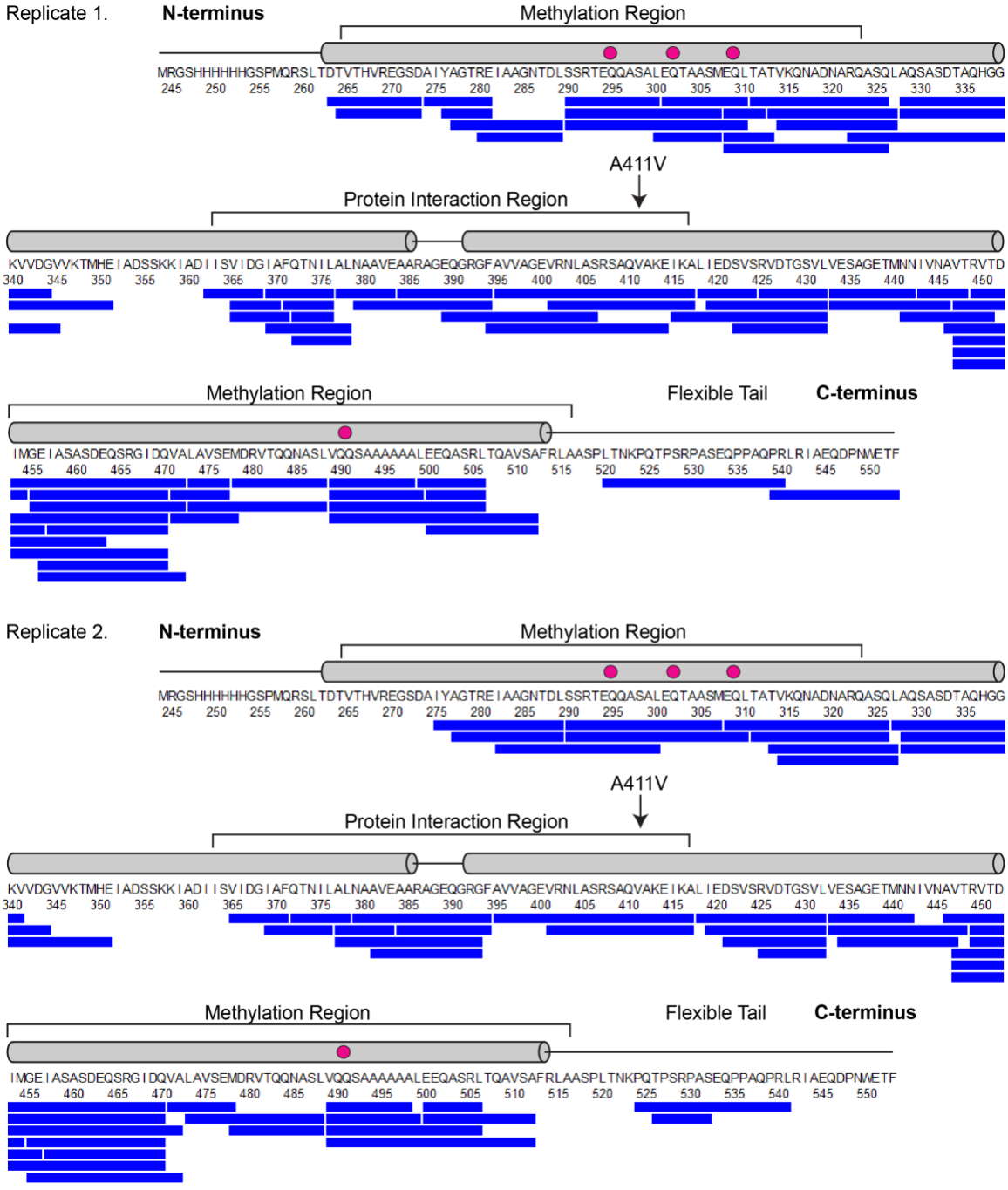

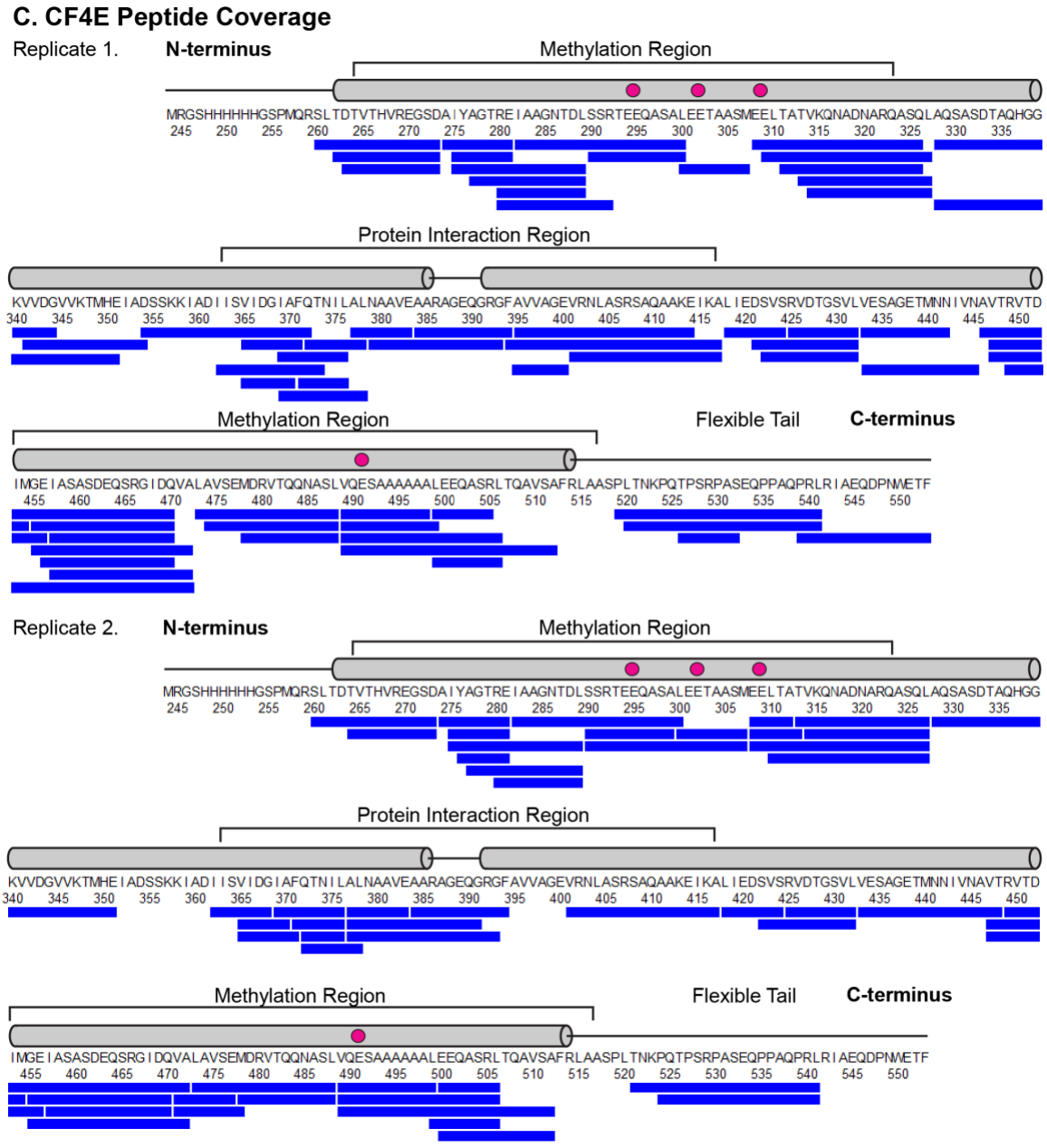

Figure 3.2. Peptide coverage maps for CF in functional complexes with CheA and CheW. Peptide numbering corresponds to the sequence of the intact *E. coli* Asp receptor. Blue bars below the sequence are CF peptides from each of two replicates for (A) CF4Q, (B) CF4Q.A411V and (C) CF4E. CF secondary structure elements and regions are labelled above the sequence, and methylation sites are shown as magenta circles. Average peptide coverage and amino acid redundancy are 80% and 3.4 for CF4Q, 83% and 3.1 for CF4Q.A411V, and 88% and 2.6 for CF4E.

3.2. Widely varying HDX rates of CF are indicative of unstructured regions and protein interactions

Figure 3.3 illustrates hydrogen exchange throughout CF4Q within functional, kinase-on complexes assembled with CheA and CheW on vesicles. The mass spectra for many peptides exhibit bimodal isotopic distributions (discussed below in section 3.5), but many key features of the exchange properties can be deduced from analysis of the centroid mass (intensity-weighted average mass). The percent deuterium uptake of each peptic peptide is calculated by subtracting the centroid mass of the undeuterated sample from that of the deuterated sample at each time point, and then dividing by the uptake of the fully deuterated control sample (complete exchange). Deuterium uptake data are shown for representative peptides showing the 80% sequence coverage (all but the black regions) in Figure 3.3A. Uptake data for the full set of all peptides from functional complexes of CF4Q, CF4Q.A411V, and CF4E, as well as CF4Q alone, are shown in Figure 3.4. In both Figures 3.3A and 3.4, blue to red rainbow colors represent 0 to 100% deuterium uptake of peptides for the 3 min to 960 min (16 hr) time points. In Figure 3.3B the exchange is visualized on the structure of a monomer of CF at both 3 min and 16 hr, using colors representing the average percent deuterium uptake for overlapping peptides (data that was averaged is indicated by boxes in Figure 3.4).

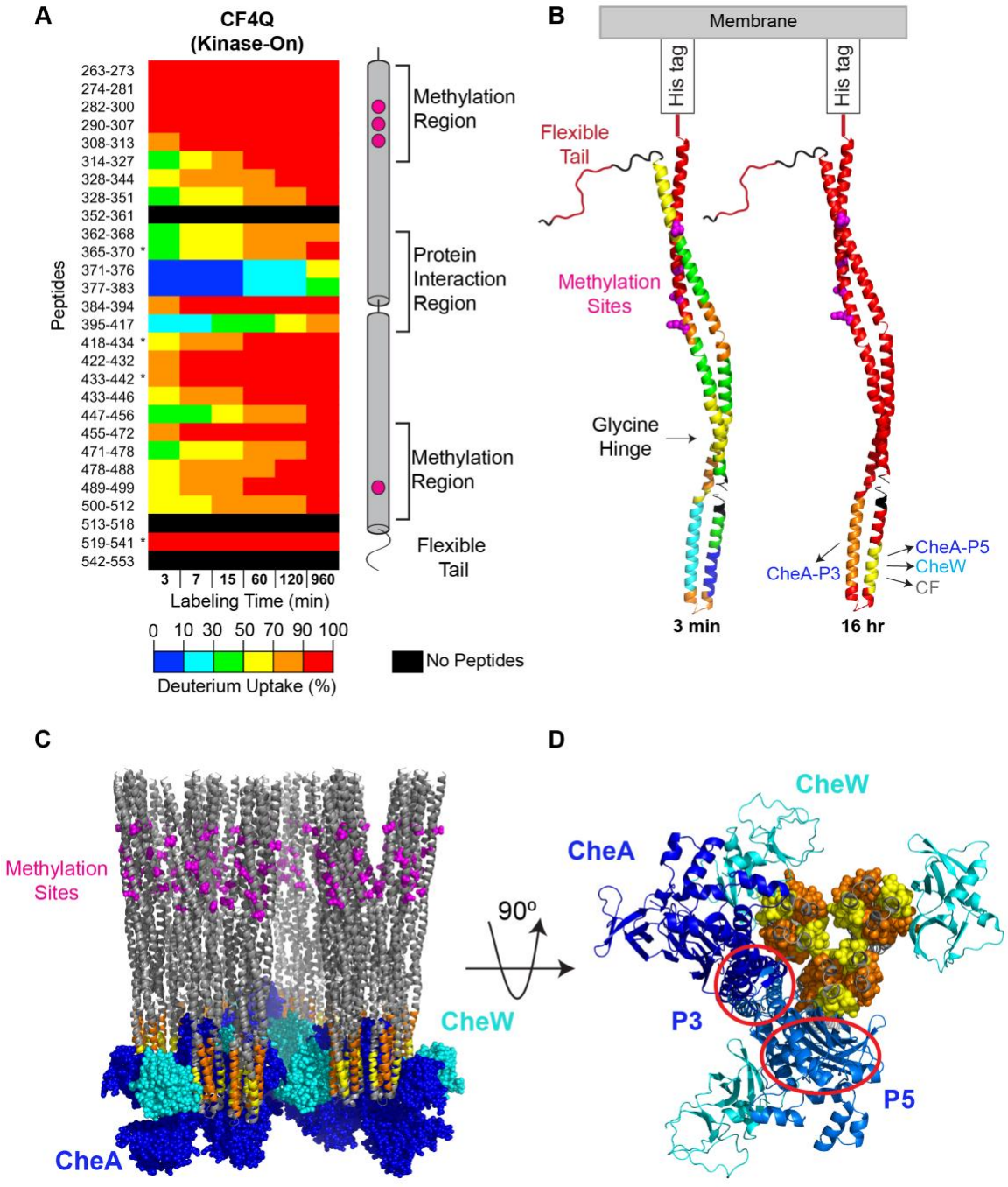
A
CF4Q
(Kinase-On)
263-273
274-281
282-300
290-307
308-313
314-327
328-344
328-351
352-361
362-368
365-370 *
371-376
377-383
384-394
395-417
418-434 *
422-432
433-442 *
433-446
447-456
455-472
471-478
478-488
489-499
500-512
513-518
519-541 *
542-553
Peptides
3 7 15 60 120 960
Labeling Time (min)
0 10 30 50 70 90 100
Deuterium Uptake (%)
Methylation Region
Protein Interaction Region
Methylation Region
Flexible Tail
No Peptides
B
Membrane
His tag
His tag
Flexible Tail
Methylation Sites
Glycine Hinge
CheA-P3
CheA-P5
CheW
CF
3 min
16 hr
C
Methylation Sites
CheW
CheA
90°
D
CheW
CheA
P3
P5

Figure 3.3. Overview of hydrogen exchange properties of CF4Q in functional complexes assembled with CheA and CheW on vesicles. (A) Deuterium uptake vs time for representative CF peptides covering the entire sequence, except segments shown in black (see Figure 3.4 for complete set of peptides, with % uptake numbers). Percent deuterium uptake of peptides at each time point is represented in rainbow colors from blue to red, indicating low to high deuterium incorporation. Data are averages of 2 replicates, except for *peptides that were not found in both data sets. Secondary structure elements of CF are shown on the right, with methylation sites (magenta) and different regions indicated. (B) CF structure is colored according to the percent deuterium uptake at the first and last time points, providing an overview of initial exchange rates (3 min) and of protection from complete exchange at long times (960 min = 16 hr). For clarity, only a monomer is shown (using PDB file 1qu7 for the Ser receptor CF). Colors are chosen based on averaging the data for overlapping peptides (see black boxes in Figure 3.4). Segments undergoing very fast exchange (complete exchange in 3 min) are the N-terminal side of the methylation region and the C-terminal tail. Segments with incomplete exchange at 16 hours correspond to sites of interactions with the indicated proteins. (C) Side and (D) bottom-up views of a structural model of functional complexes of CF, CheA, and CheW. CF is colored gray, except peptides showing protection at 16 hr are colored as in (B). The orange peptide (395-417) is at the interface with the P3 dimerization domain of CheA (red circle). The yellow peptides (371-376, 377-383) are at the interface with the P5 domain of CheA (red oval), or with CheW (cyan), or with another CF dimer in the center of the receptor trimer-of-dimers. Peptide numbering corresponds to the sequence of the intact *E. coli* Asp receptor. Model of complex shown in C and D is based on the array model of Briegel, Crane, and Jensen (Briegel et al., 2012) with an additional CheW positioned via superposition of the neighboring CF dimer tip with the array model 3AJ6 (Cassidy et al., 2015).

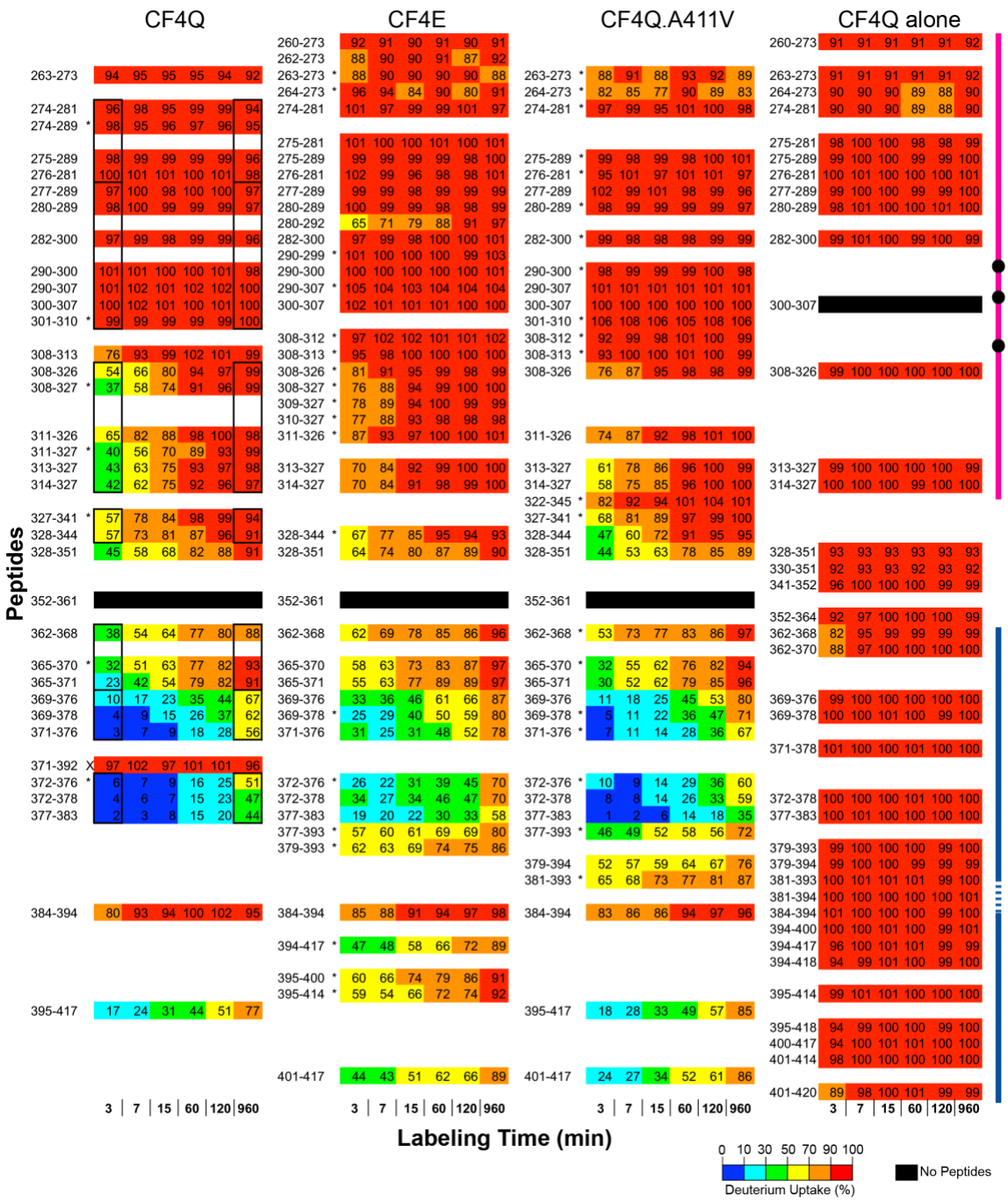
CF4Q
CF4E
CF4Q.A411V
CF4Q alone
Peptides
Labeling Time (min)
3 | 7 | 15 | 60 | 120 | 960
0 10 30 50 70 90 100
Deuterium Uptake (%)
No Peptides

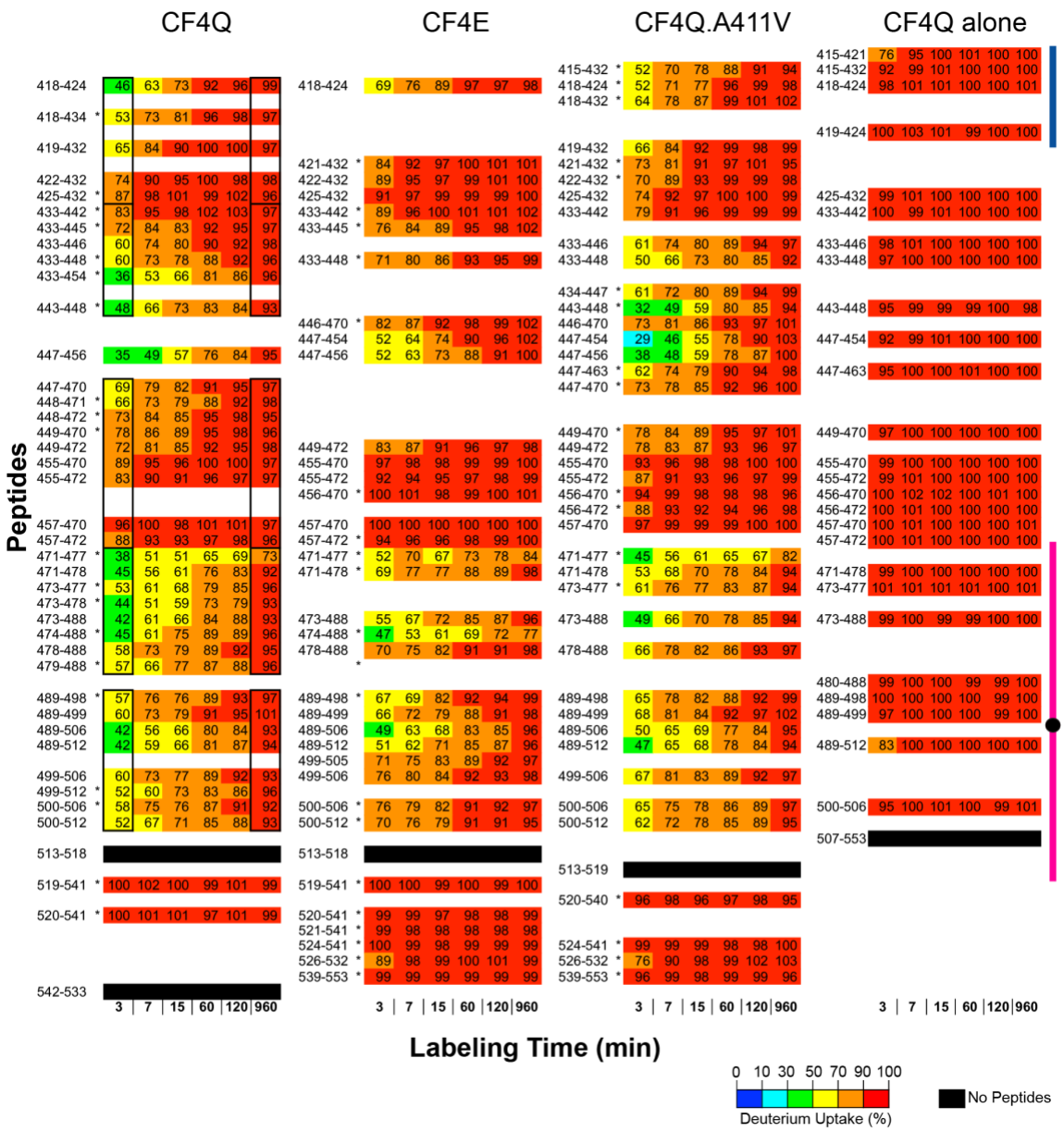
CF4Q
CF4E
CF4Q.A411V
CF4Q alone
Peptides
Labeling Time (min)
3 | 7 | 15 | 60 | 120 | 960
0 10 30 50 70 90 100
Deuterium Uptake (%)
No Peptides

Figure 3.4. Hydrogen exchange for the complete set of CF peptides from CF4Q, CF4E, and CF4Q.A411V in functional complexes with CheA and CheW, and from CF4Q alone. A subset of the CF4Q data are shown in Figure 3.3. Percent deuterium uptake is calculated based on a centroid analysis, as the uptake of the peptide at each time point divided by the uptake of the fully exchanged sample, and is represented with both numbers and rainbow colors from blue to red for low to high uptake. Regions where no peptides were observed are shown in black. Peptides with asterisks were found in a single data set; others were found in both replicates. Finally, X marks an outlier peptide (371-392) that we neglected in the analysis because a single replicate for a single state was observed and its rapid exchange was inconsistent with the slow exchange of six overlapping peptides. Uptake for overlapping peptides outlined by black boxes was averaged to choose colors represented on Figure 3.3 for 3 min and 16 hourHDX. Note that for the CF4Q alone sample, nearly all peptides exhibit ≥ 90% exchange (red) within 3 min. The few time points that show 70-90% exchange (orange) all have at least one overlapping peptide with ≥ 90% exchange (or 88% exchange for residues 365-368). Thus, we conclude that the entire CF alone sample exhibits very rapid exchange (≥ 90% within 3 min). Vertical lines on the right side of the figure represent regions of the CF: magenta lines indicate the methylation region, with methylation sites shown as black circles; blue lines indicate the protein interaction region, with the membrane-distal hairpin tip of the receptor shown as a dashed line.

The initial deuterium uptake for the first 3 min time point (Fig 3.3A & B) varies widely from >90% (red) near the N and C termini to <10% (blue) near the membrane-distal tip. Peptides near the N and C termini exhibit very fast exchange, with 90-100% deuterium uptake in the first 3 minutes, suggesting these regions are highly flexible and solvent exposed. These findings are consistent with previous hydrogen exchange mass spectrometry (Koshy et al., 2014) and NMR INEPT studies (Kashefi and Thompson, 2017) on similar samples of functional complexes, and with electron paramagnetic resonance (EPR) on spin labelled intact receptors in nanodiscs (Bartelli and Hazelbauer, 2016). The C-terminal tail is thought to be an unstructured, flexible tether for binding the methylation and demethylation enzymes. The comparably rapid hydrogen exchange observed for residues 263-307, near the membrane-anchored N-terminal His tag (residues 248-253), suggests that this is also an unstructured, flexible segment.

The slowest hydrogen exchange occurs near the membrane-distal cytoplasmic tip of the CF, in the protein interaction region. With the exception of the 384-394 peptide at the hairpin tip of the CF, which exhibits rapid exchange (80% at 3 min), residues 369–417 exhibit only 2–17% exchange in the first 3 minutes (neglecting the outlier behavior of the 371-392 peptide, marked X as discussed in Figure 3.4 legend). The slow exchange in this region (both sides of hairpin tip) continues throughout the time course, resulting in incomplete exchange at the final time point (16 hours) for these peptides. This slow exchange and protection from complete exchange is likely due to protein-protein interactions in this region, as illustrated in Figures 3.3C and 3.3D, which show a structural model of the CF array (Briegel et al., 2012), with the regions protected from complete exchange colored by their uptake at 16 hours (as in Figure 3.3B) and the rest of the CF colored gray. The 369-383 region (yellow) is involved in protein interactions with the P5 domain of CheA (red oval), with CheW (homologous to P5), and with CF at the center of the trimer-of-dimers. Similarly, the 395-417 region (orange) is involved in protein interactions with the P3 dimerization domain of CheA (red circle).

For comparison, the hydrogen exchange time course for CF4Q alone (in the absence of vesicles, CheA and CheW; right column in Figure 3.4) shows ≥88% exchange throughout the protein in 3 minutes and no protection in the protein interaction region at 16 hours. Interestingly, one peptide outside of the protein interaction region (328–351) exhibits incomplete exchange at a significant level (1.6–1.9 Da) in functional complexes of CF4Q, CF4E, and CF4Q.A411V, and also in CF4Q alone (1.4 Da unexchanged at 16 hours for peptides 328–351 and 330–351). As explained in the Methods section, differences greater than 0.9 are judged to be significant. Note that 1.9 Da is < 10% for these

long peptides, so the final time points in Figure 3.4 show ≥ 90% exchange. Thus, we conclude that incomplete exchange in the 328–351 region is an intrinsic property of the CF protein itself, and all other sites of incomplete exchange in CF complexes localize to the protein interaction region.

The overall properties observed for the kinase-on arrays of CF4Q, extremely rapid exchange for peptides near the N and C termini and slow exchange for peptides in the protein interaction region (with the exception of the hairpin tip itself), are also observed in functional arrays of CF4Q.A411V (kinase-off mutant) and CF4E (other methylation extreme). Furthermore, in all regions other than the protein interaction sites where incomplete exchange at 16 hours is observed, HDX is rapid (≥50% by 15 min). Thus, within all three types of functional complexes, the majority of the CF is dynamic. Although these overall HDX properties are similar for all three types of complexes (see Figure 3.4), there are subtle differences in hydrogen exchange with signaling state and methylation state, which are described in the next two sections (3.3-3.4). Interestingly, all of the functional complexes also exhibit widespread bimodal isotope distributions, which will be reported in the final section of this chapter (3.5).

3.3. CF in the kinase-on state exhibits decreased dynamics in both the methylation and protein interaction regions

The differences in the deuterium uptake time course of the kinase-on (CF4Q) and kinase-off (CF4Q.A411V) functional complexes is illustrated in Figure 3.5. Differences in uptake are indicated by colors for representative peptides in Figure 3.5A: blue colors indicate peptides with slower HDX in the kinase-on state; red colors indicate peptides with

faster HDX in the kinase-on state. Light gray indicates no significant difference in uptake ($\leq \pm 0.9$ Da (Houde et al., 2011)). Dark gray indicates very fast exchange ($\geq 90\%$ in 3 min), so our HDX-MS experiment does not have the time resolution to detect the differences between the two states for these peptides. Black indicates no peptides found for these regions. Two replicates were averaged for each type of complex, except each * indicates a missing replicate. Secondary structure elements of CF are shown on the right side of Fig 3.5A, with methylation sites (magenta) and different regions indicated. In Figure 3.5B the difference in uptake is visualized on the structure of a monomer of CF at 3 min and 16 hr, using colors representing the average difference in deuterium uptake for overlapping peptides (see boxes in Figure 3.7 below, which includes the uptake difference data for the full set of observed peptides).

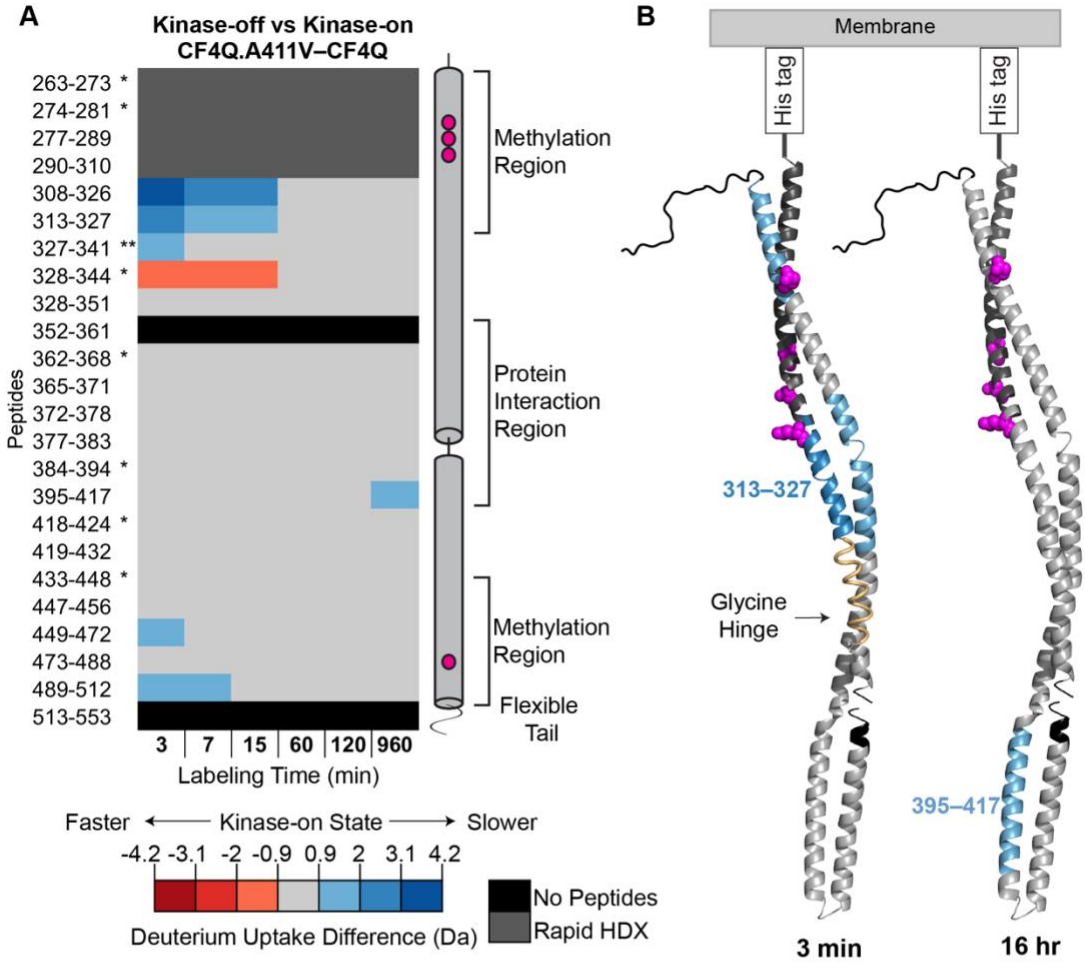
A
Kinase-off vs Kinase-on
CF4Q.A411V–CF4Q
263-273 *
274-281 *
277-289
290-310
308-326
313-327
327-341 **
328-344 *
328-351
352-361
362-368 *
365-371
372-378
377-383
384-394 *
395-417
418-424 *
419-432
433-448 *
447-456
449-472
473-488
489-512
513-553
Peptides
Methylation Region
Protein Interaction Region
Methylation Region
Flexible Tail
3 7 15 60 120 960
Labeling Time (min)
Faster ← Kinase-on State → Slower
-4.2 -3.1 -2 -0.9 0.9 2 3.1 4.2
Deuterium Uptake Difference (Da)
No Peptides
Rapid HDX
B
Membrane
His tag
His tag
313–327
Glycine Hinge
395–417
3 min
16 hr

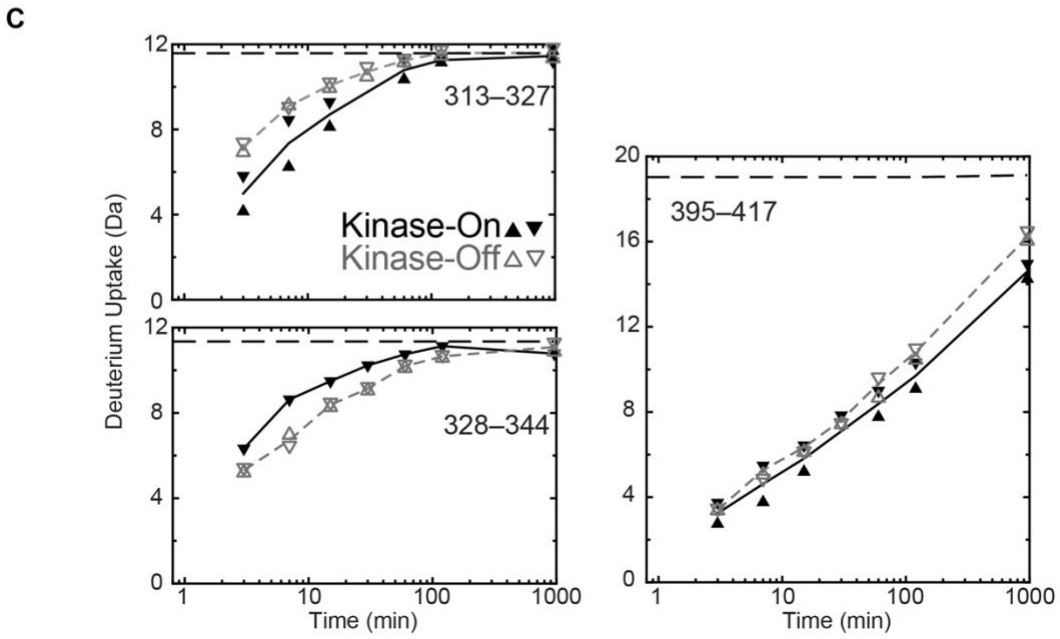
C
313–327
Kinase-On▲▼
Kinase-Off△▽
328–344
Deuterium Uptake (Da)
Time (min)
395–417
Time (min)

Figure 3.5. Difference in deuterium uptake between kinase-on and kinase-off signaling states. (A) Deuterium uptake of kinase-off CF4Q.A411V minus kinase-on CF4Q, for representative CF peptides covering the entire sequence, except segments shown in black (see Figure 3.7 for complete set of peptides). Segments in dark gray undergo very fast exchange (≥ 90% in 3 min), so these HDX experiments do not have the time resolution to detect differences between the two states in these regions. Segments in blue colors undergo slower HDX in the kinase-on state; segments in red colors undergo faster HDX in the kinase-on state; segments in light gray show no significant difference in uptake (difference ≤ ±0.9 Da). Uptake differences are computed from averages of 2 replicates for each state, except for *peptides that were missing in one data set, and ** peptides that were missing in 2 of the 4 data sets. (B) CF monomer structure (PDB file 1qu7 for Ser receptor CF, with methylation sites shown as magenta spheres) is colored according to the difference in deuterium uptake between the kinase-on and kinase-off states at the first (3 min) and last (16 hr) time points. For overlapping peptides, colors were chosen based on averaging the data for peptides showing significant uptake differences (see black boxes in Figure 3.7). Light yellow loop on 3 min structure encloses a region that shows conflicting data, with the 327-344 peptide showing slower HDX and the 328-344 peptide showing faster HDX in the kinase-on state. (C) Plots of deuterium uptake vs time for representative peptides of both CF4Q (black symbols and solid lines) and CF4Q.A411V (gray symbols and dashed lines). Data points for all replicates are shown, along with lines connecting the averages of the replicates for each sample type. Dashed horizontal lines near top of plots indicate the deuterium level expected for complete exchange, based on control samples of CF subjected to reversible heat denaturation in D_2O buffer followed by the quench and mass spectrometry protocol used for all HDX samples.

Several peptides on the N and C terminal sides of the methylation region exhibit slower initial exchange in the kinase-on state, as shown by blue colors for early time points in Figure 3.5A and blue color in the top half of the structure in Figure 3.5B. Figure 3.5C includes the uptake plot for one of these peptides, 313-327, which shows an initial difference in uptake that disappears at long times as the data approach complete exchange (dashed line is uptake level of completely-exchanged control). This suggests that the methylation region is less dynamic in the kinase-on state. Note that the N-terminal side of the methylation region exchanges too quickly for detection of differences in HDX (exchange complete in 3 min), but a recent INEPT NMR study (Kashefi and Thompson, 2017) of this segment within similar functional complexes indicates that the kinase-off state is more dynamic. There is also one region of the C-terminal side of the methylation

region (473-488) exhibits no significant differences in HDX. With the exception of these regions, the entire methylation region exhibits less uptake at early times in the kinase-on state. This observation is consistent with a previous hydrogen exchange mass spectrometry study (Koshy et al., 2014)on similar samples of functional complexes.

Interestingly, an opposite change in dynamics is observed in a single peptide in the glycine hinge region on the N-terminal side of the CF: peptide 328-344 (red color in Figure 3.5A and light yellow loop in Figure 3.5B) exhibits faster deuterium uptake (plotted in Figure 3.5C) in the kinase-on state. This change is only observed in the 328-344 peptide; the overlapping 328-341 peptide shows the opposite change (slower uptake at 3 min). For analysis of differences in HDX between states (Figures 3.5-3.7), we have averaged the data for the overlapping peptides with significant differences. This results in this region having no significant difference, as indicated by the light yellow color on the structure in Figure 3.5B. However, the data for the 328-344 peptide (see plot in Figure 3.5C) may be more reliable than that of the 328-341 peptide, because the 328-344 peptide has one additional replicate and the difference in initial HDX is observed for more time points. Thus, we have included the light yellow on the structure in Figure 3.5B to indicate the possibility that this segment experiences faster HDX in the kinase-on state.

At the 16 hr time point, a single peptide in the protein interaction region shows a significant difference in exchange. Peptide 395–417, on the C-terminal side of the hairpin tip, shows incomplete exchange in both CF4Q (4.4 Da) and CF4Q.A411V (2.8 Da). These data indicate significantly less deuterium uptake (1.6 Da) in the CF4Q kinase-on state, as represented by the blue color in Fig 3.5A-B and the difference in the uptake plot at long times in Figure 3.5C. This peptide, at the protein interface between CF and CheA-P3 (see

Fig 3.3D), also contains the A411V mutation that creates the kinase-off state. We suggest that that the kinase-off state has a decreased affinity for CheA-P3, which decreases the protection from complete HDX at long times. Such a decrease in affinity does not result in a greater loss of bound CheA from the complexes with time (Table 3.1), perhaps reflecting the high stability of the overall CheA/CheW hexagonal network of the array. Interestingly, the other peptides of the protein interaction region that show protection at long times (N-terminal side of the hairpin tip: 369-376, see Figure 3.4) show no significant differences in uptake between the kinase-on and kinase-off states.

Finally, although the HDX differences between the kinase-on CF4Q and kinase-off CF4Q.A411V are subtle, they demonstrate long-range coupling: differences are observed in both the methylation region at early times and in the protein interaction region near the kinase-off mutation site at long times. This is consistent with the fact that the A411V mutation causes both inactivation of the kinase (a local change in the CF-CheA interaction) and activation of methylation (a long-range change in the CF), and suggests that both of these activity changes are correlated with increased dynamics of the CF.

3.4. Methylation decreases dynamics throughout the CF

In contrast to the subtle differences in HDX between the kinase-on and kinase-off states, methylation has a much greater effect on the CF dynamics. Figure 3.6 illustrates the difference in deuterium uptake between unmethylated (CF4E) and methylated-mimic (CF4Q) functional complexes assembled with CheA and CheW on vesicles. As in Figure 3.5, the uptake differences are computed between average of two replicates for each state (except for peptides marked by * or **), with light gray indicating no significant difference in uptake ($\leq \pm 0.9$ Da) and dark gray indicating very fast exchange ($\geq 90\%$ in 3 min), so

differences cannot be measured by our experiments. Difference uptake data for representative peptides covering the sequence are shown in Figure 3.6A, with data for the full set of observed peptides shown in Figure 3.7. Blue colors, indicating peptides with slower HDX in the CF4Q methylated-mimic state, are observed throughout the CF at short times and in the protein interaction region at long times. Again, the colors shown on the structure (Figure 3.6B) represent the average difference in deuterium uptake for overlapping peptides (boxes in Figure 3.7 indicate which data were averaged).

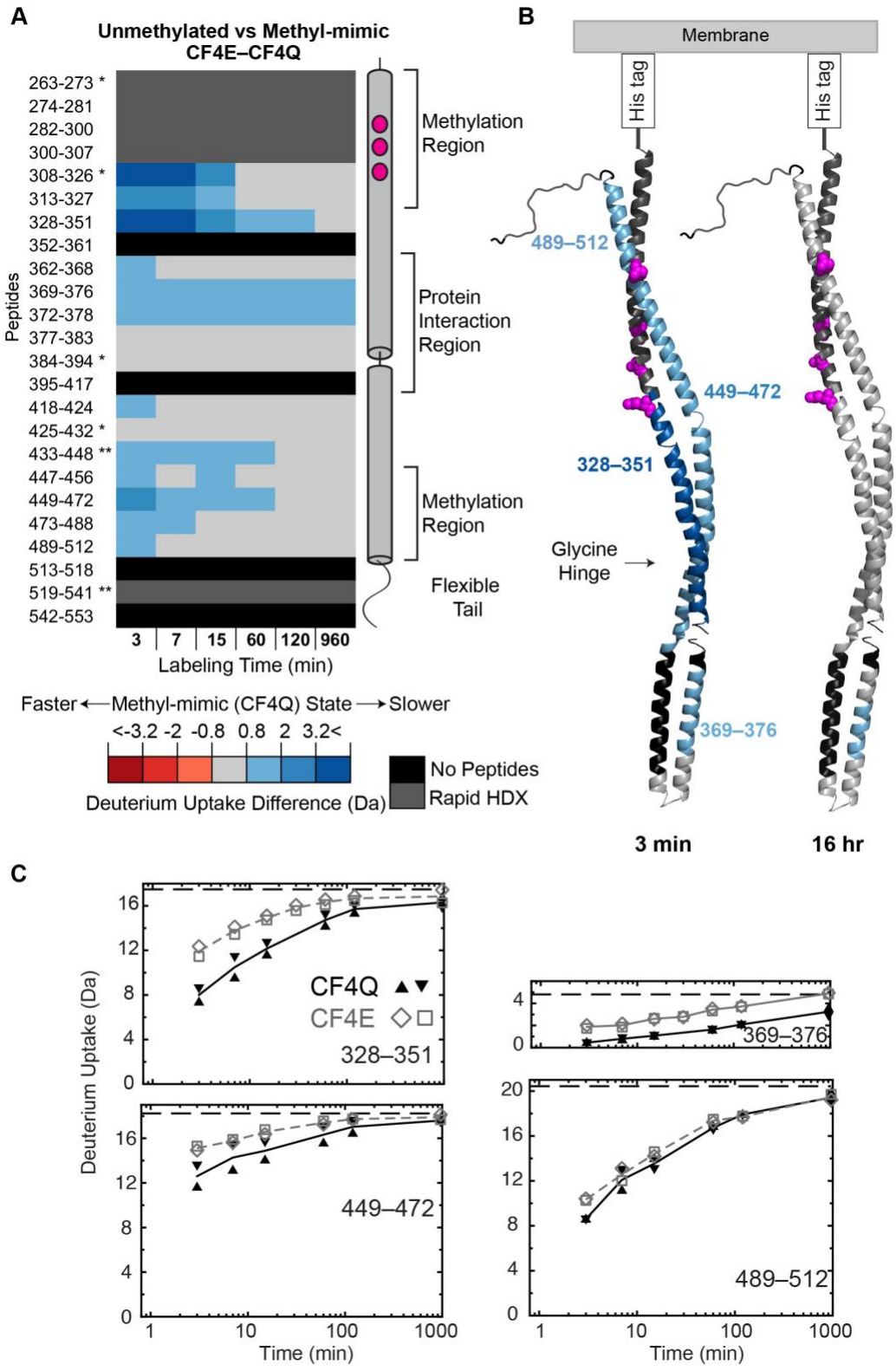
A
Unmethylated vs Methyl-mimic
CF4E–CF4Q
263-273 *
274-281
282-300
300-307
308-326 *
313-327
328-351
352-361
362-368
369-376
372-378
377-383
384-394 *
395-417
418-424
425-432 *
433-448 **
447-456
449-472
473-488
489-512
513-518
519-541 **
542-553
Peptides
3 7 15 60 120 960
Labeling Time (min)
Methylation Region
Protein Interaction Region
Methylation Region
Flexible Tail
Faster ← Methyl-mimic (CF4Q) State → Slower
<-3.2 -2 -0.8 0.8 2 3.2<
Deuterium Uptake Difference (Da)
No Peptides
Rapid HDX
B
Membrane
His tag
His tag
489–512
449–472
328–351
Glycine Hinge
369–376
3 min
16 hr
C
Deuterium Uptake (Da)
CF4Q
CF4E
328–351
449–472
369–376
489–512
Time (min)
Time (min)

Figure 3.6. Difference in deuterium uptake between unmethylated and methylated-mimic states. (A) Deuterium uptake of unmethylated CF4E minus methylated-mimic CF4Q for representative CF peptides covering the entire sequence, except segments shown in black (see Figure 3.7 for complete set of peptides). Segments in dark gray undergo very fast exchange (≥90% in 3 min), so these HDX experiments do not have the time resolution to detect differences between the two states in these regions. Segments in blue colors undergo slower HDX in the methylated-mimic state; segments in light gray show no significant difference in uptake (different ≤ ±0.9 Da). Uptake differences are computed from averages of 2 replicates for each state, except each asterisk indicates one missing replicate (** indicates peptide is observed in only 2 of the 4 data sets). (B) CF monomer structure (Ser receptor CF PDB file 1qu7, with methylation sites shown as magenta spheres) is colored according to the difference in deuterium uptake between the unmethylated and methylated-mimic states at the first (3 min) and last (16 hr) time points. For overlapping peptides, colors were chosen based on averaging the data for peptides showing significant uptake differences (see black boxes in Figure 3.7). (C) Plots of deuterium uptake vs time for representative peptides of both CF4Q (black symbols and solid lines) and CF4E (gray symbols and dashed lines). Data points for all replicates are shown, along with lines connecting the averages of the replicates for each sample type. Dashed horizontal lines near top of plots indicate the deuterium level expected for complete exchange, based on control samples of CF subjected to reversible heat denaturation in D_2O buffer followed by the quench and mass spectrometry protocol used for all HDX samples.

At early times, peptides throughout the methylation, glycine hinge and protein interaction regions exhibit slower exchange in the CF4Q methylated-mimic state (Fig 3.6A, B & C). In fact, of the regions with measurable HDX rates, nearly all contain at least one peptide that shows significantly less deuterium uptake in CF4Q. The single exception is the 379-394 region, which is likely dominated by the properties of the hairpin tip peptide, 384-394, that exhibits fairly rapid exchange in all complexes. Thus, we conclude that methylation causes widespread stabilization (resulting in slower initial HDX) throughout all of the CF except for the hairpin tip and the rapidly exchanging N and C-terminal regions.

At long times (16 hr), peptides involved in protein interactions (those that show incomplete exchange) exhibit reduced uptake in the methylated-mimic state. This is observed on the N-terminal side of the hairpin tip (369-378, which interacts with CheA-P5/CheW/CF as shown in Figure 3.3). Unfortunately, the peptide involved in protein

interactions on the C-terminal side (395-417) is missing in the CF4E data set, so we cannot determine whether it too would show decreased uptake at long times in CF4Q relative to CF4E. Although it is not clear whether methylation alters CF interactions with CheA-P3, it appears that methylation increases the affinity of CF interactions with CheA-P5 and/or CheW and/or other CF dimers in the trimer of dimers. Overall, these HDX data suggest that methylation causes widespread stabilization of CF and its interactions. It is not clear why the uptake differences due to signaling state (Figure 3.7A) are much more limited than the uptake differences due to methylation state (Figure 3.7B).

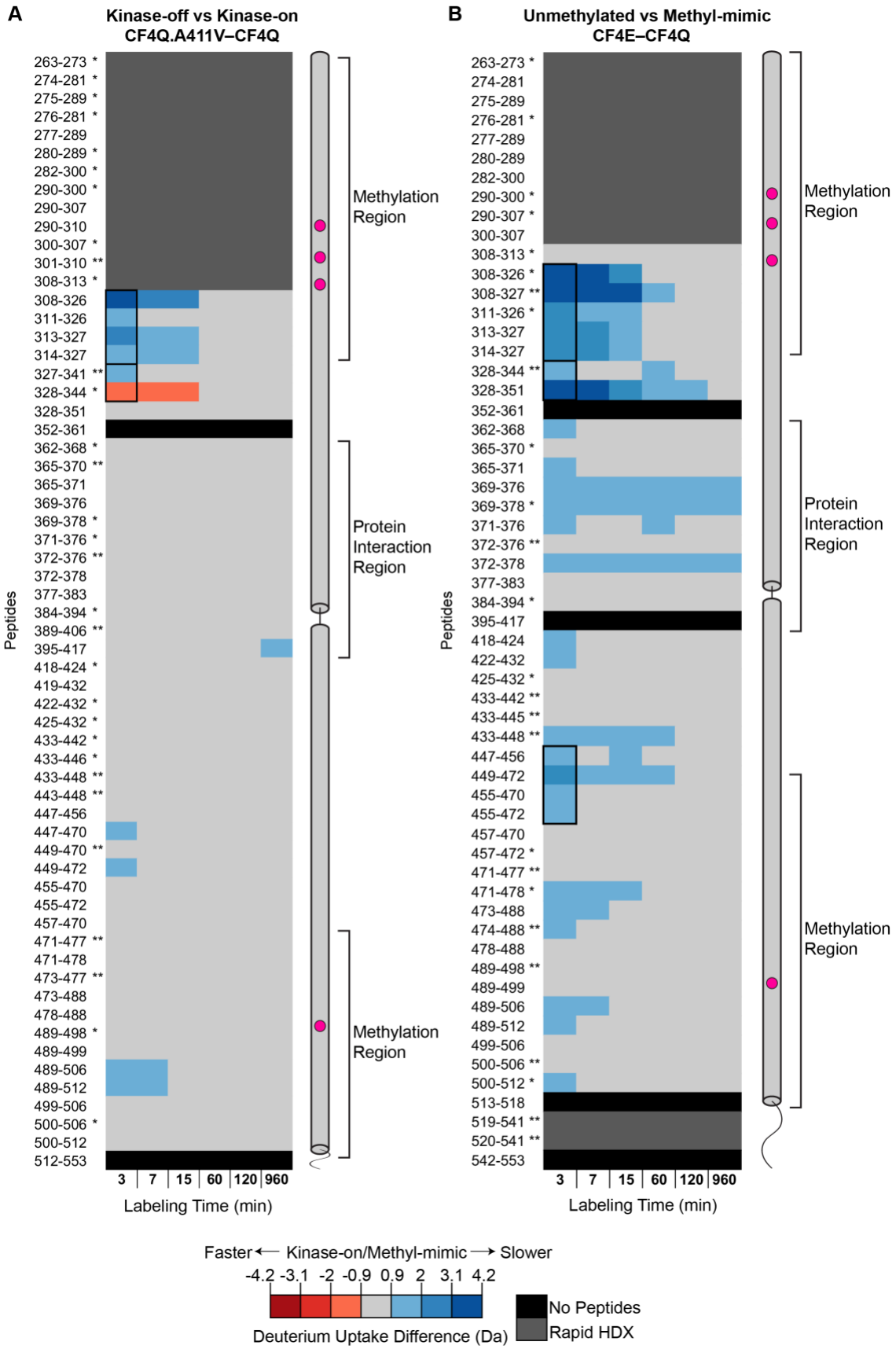
A
Kinase-off vs Kinase-on
CF4Q.A411V–CF4Q
B
Unmethylated vs Methyl-mimic
CF4E–CF4Q
Peptides
263-273 *
274-281 *
275-289 *
276-281 *
277-289
280-289 *
282-300 *
290-300 *
290-307
290-310
300-307 *
301-310 **
308-313 *
308-326
311-326
313-327
314-327
327-341 **
328-344 *
328-351
352-361
362-368 *
365-370 **
365-371
369-376
369-378 *
371-376 *
372-376 **
372-378
377-383
384-394 *
389-406 **
395-417
418-424 *
419-432
422-432 *
425-432 *
433-442 *
433-446 *
433-448 **
443-448 **
447-456
447-470
449-470 **
449-472
455-470
455-472
457-470
471-477 **
471-478
473-477 **
473-488
478-488
489-498 *
489-499
489-506
489-512
499-506
500-506 *
500-512
512-553
Methylation Region
Protein Interaction Region
Methylation Region
263-273 *
274-281
275-289
276-281 *
277-289
280-289
282-300
290-300 *
290-307 *
300-307
308-313 *
308-326 *
308-327 **
311-326 *
313-327
314-327
328-344 **
328-351
352-361
362-368
365-370 *
365-371
369-376
369-378 *
371-376
372-376 **
372-378
377-383
384-394 *
395-417
418-424
422-432
425-432 *
433-442 **
433-445 **
433-448 **
447-456
449-472
455-470
455-472
457-470
457-472 *
471-477 **
471-478 *
473-488
474-488 **
478-488
489-498 **
489-499
489-506
489-512
499-506
500-506 **
500-512 *
513-518
519-541 **
520-541 **
542-553
Methylation Region
Protein Interaction Region
Methylation Region
3 7 15 60 120 960
Labeling Time (min)
3 7 15 60 120 960
Labeling Time (min)
Faster ← Kinase-on/Methyl-mimic → Slower
-4.2 -3.1 -2 -0.9 0.9 2 3.1 4.2
Deuterium Uptake Difference (Da)
No Peptides
Rapid HDX

Figure 3.7. Comparison of HDX differences due to signaling state and methylation. For complete set of CF peptides, colors indicate deuterium uptake differences between kinase-on/methyl-mimic (CF4Q) and (A) kinase-off (CF4Q.A411V) or (B) unmethylated (CF4E) states. A subset of the data shown in (A) are presented in Figure 3.5; a subset of the data shown in (B) are presented in Figure 3.6. Segments in dark gray undergo very fast exchange ($\geq$ 90% in 3 min), so these HDX experiments do not have the time resolution to detect differences between the two states in these regions. Segments in blue colors undergo slower HDX in the CF4Q kinase-on state; segments in red colors undergo faster HDX in the CF4Q kinase-on state; segments in light gray show no significant difference (difference $\leq \pm 0.9$ Da). Single asterisks indicate the peptide is observed in only 3 of the 4 data sets (two replicates for each sample type). Two asterisks indicate the peptide is observed in only 2 of the 4 data sets. In both (A) and (B), black boxes for the 3 min time points enclose overlapping peptides that were averaged to determine the color represented on the structures in Figures 3.5 and 3.6.

3.5. Widespread correlated exchange suggests CF populates a long-lived unfolded state within functional complexes

In these HDX experiments, HDX data for many peptides exhibit bimodal isotopic distributions, with one isotopic distribution at low m/z that moves gradually to higher mass with time (uncorrelated exchange), and another isotopic distribution at the final exchange m/z positon that increases in intensity with time (correlated exchange). Uncorrelated exchange is often observed in proteins under native conditions, where the refolding rate of the protein is faster than the exchange, so the protein must undergo multiple unfolding and refolding events before HDX is complete. Correlated exchange is observed when the protein refolding rate is slower than the exchange (known as the EX1 limit): there is a long-lived unfolded state which undergoes complete exchange before refolding. Although the HDX patterns observed for CF include bimodal patterns indicative of correlated exchange (EX1), the deuterium uptake analysis of the HDX data described thus far was performed with the instrument software, which calculates the centroid of each spectrum (intensity-weighted mass average) and thus ignores the bimodal patterns and the underlying EX1

process. We pursued additional analysis of these bimodal patterns to gain insight into the long-lived unfolded state and how it relates to methylation and signaling states.

Peptides with HDX mass spectra with bimodal distributions are observed throughout the CF in all functional complexes with CheA and CheW. However, the HDX spectra do not follow an idealized EX1 pattern, with mass envelopes only at zero exchange and complete exchange. Instead a simultaneous uncorrelated exchange occurs, as expected for "realistic" EX1 (Xiao et al., 2005): the lower m/z envelope shifts gradually to higher m/z, merging with the envelope at the fully exchanged position. A detailed deconvolution analysis of these data would be challenging due to the large number of peptides and the incomplete resolution of the bimodal distributions for many cases. We implemented an efficient method to estimate $t_{1/2}$ of the correlated exchange process (EX1) for each peptide that exhibited HDX with bimodal isotopic distributions. Since correlated exchange populates the fully exchanged isotopic distribution (at high m/z), this process reaches 50% completion when this high m/z mass envelope contains 50% of the intensity in the spectrum. Thus, at $t_{1/2}$ for the EX1 process the bimodal distribution should be symmetric, with equal intensities in the mass envelopes at the low m/z position and at the fully exchanged position. The symmetry of the pattern is an especially useful indicator when the mass envelopes have merged, at which point it is difficult to estimate the intensity in the high m/z mass envelope.

To validate our method, we compare the $t_{1/2}$ values estimated visually with the results of deconvolution analysis with HX-Express. Figure 3.8 shows the mass spectra for the HDX time course of two peptides in each of the three types of functional CF complexes, and compares the visual estimate of $t_{1/2}$ (top) with the deconvolution method (bottom). For

each HDX time course (vertical series of spectra) the spectrum shown in red is the first one with ≥50% intensity in the high m/z mass envelope and/or the most symmetric pattern, indicating $t_{1/2}$ has been reached. HX-Express deconvolutes bimodal patterns into two binomial distributions, and the resulting intensity of the high m/z distribution should be 50% at the $t_{1/2}$ for the EX1 process. The deconvolution results are listed below each series of spectra, with red highlighting the first spectrum with ≥50% intensity in the high m/z mass envelope. The results of the deconvolutions demonstrate that the estimated $t_{1/2}$ using our visualization method (Figure 3.8 top) is in good agreement with the HX-Express deconvolution results (Figure 3.8 bottom).

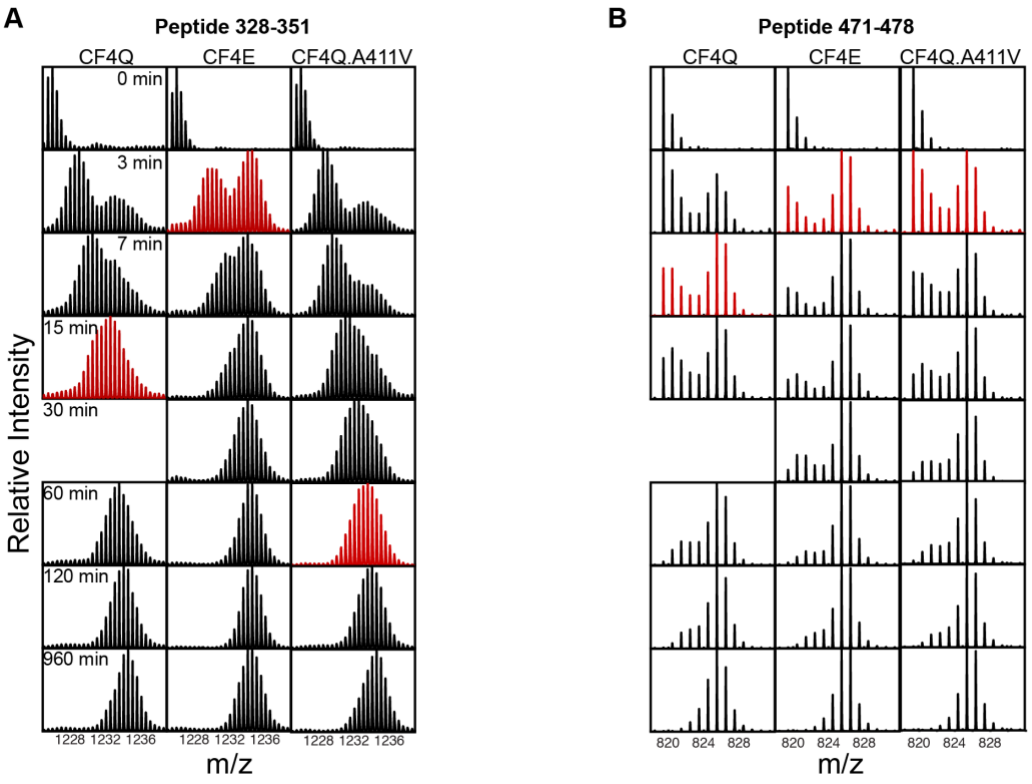

Relative intensity of high m/z distribution, based on HX-Express deconvolutions.

Peptide 328-351	Peptide 471-478

Time (min)	CF4Q	CF4E	CF4Q.A411V	CF4Q	CF4E	CF4Q.A411V
3	0.20	0.55	0.32	0.46	0.72	0.56
7	0.29	0.66	0.29	0.52	0.78	0.64
15	0.34	0.46	0.34	0.6	0.76	0.69
30	NA	0.81	0.42	NA	0.74	0.78
60	NA	0.84	0.54	0.69	0.84	0.84
120	NA	0.96	0.75	0.76	0.84	NA

Figure 3.8. Comparison of visualization *vs* HX-Express methods for estimation of $t_{1/2}$ of an EX1 process. Both methods are applied to two example peptides (A) 328-351 and (B) 471-478 that exhibit bimodal isotopic distributions during HDX. Visualization method (top): stacked spectra are used to estimate $t_{1/2}$ for the correlated exchange (EX1) process in CF4Q, CF4E and CF4Q.A411V arrays. The first spectrum with at least 50% intensity in the high m/z distribution or a symmetric pattern is highlighted in red and represents the visually estimated $t_{1/2}$ of the EX1 process. HX Express method (bottom): HX Express is used to deconvolute the bimodal patterns into two binomial distributions. The fractional intensity of the high m/z distribution at each time point is listed in the table; $t_{1/2}$ is the time at which this intensity reaches 0.5. N.A indicates either missing data or that the two binomial distributions are merged and cannot be deconvoluted. The two methods yield similar estimates; the visualization method has the advantages of being faster and applicable to spectra that lack resolution of the two distributions.

Visual estimates of $t_{1/2}$ were performed for all peptides that exhibit a significant widening of the isotopic distribution during the HDX time course. It has been previously demonstrated that a widening of 6 Da is indicative of an underlying EX1 process (Weis et al., 2006). The resulting estimated values of $t_{½}$ for correlated exchange are shown in Figure 3.9A for the three types of functional complexes of CF with CheA and CheW. The estimated values of $t_{1/2}$ for all CF peptides are represented in colors ranging from dark maroon for short $t_{1/2}$ (rapid correlated HDX) to pale purple for long $t_{1/2}$ (slow correlated HDX). Our experiments do not have the time resolution to distinguish correlated vs uncorrelated exchange for peptides that undergo very fast exchange (>70% exchange within 3 min); these peptides are shown in dark gray. Light gray indicates peptides that display only uncorrelated exchange (< 6 Da widening of isotopic distribution); black indicates regions with no peptide coverage. An average $t_{1/2}$ estimate was calculated for

overlapping peptides (black boxes in Figure 3.9A) and represented with the corresponding color on the CF monomer structures in Fig 3.9B. For the 369-378 region, we considered the fact that correlated exchange is more difficult to resolve for short peptides (eg. HDX for 2 peptides of 4-5 amino acids appears to be uncorrelated), and thus we used the $t_{½}$ estimate of 120 min consistently observed for the three longer peptides (6-8 amino acids) in this region. Figure 3.9B represents these colors on the CF structure to compare the correlated exchange profile of CF4Q (left, which is very similar to that of CF4Q.A411V) to the correlated exchange profile of CF4E (right).

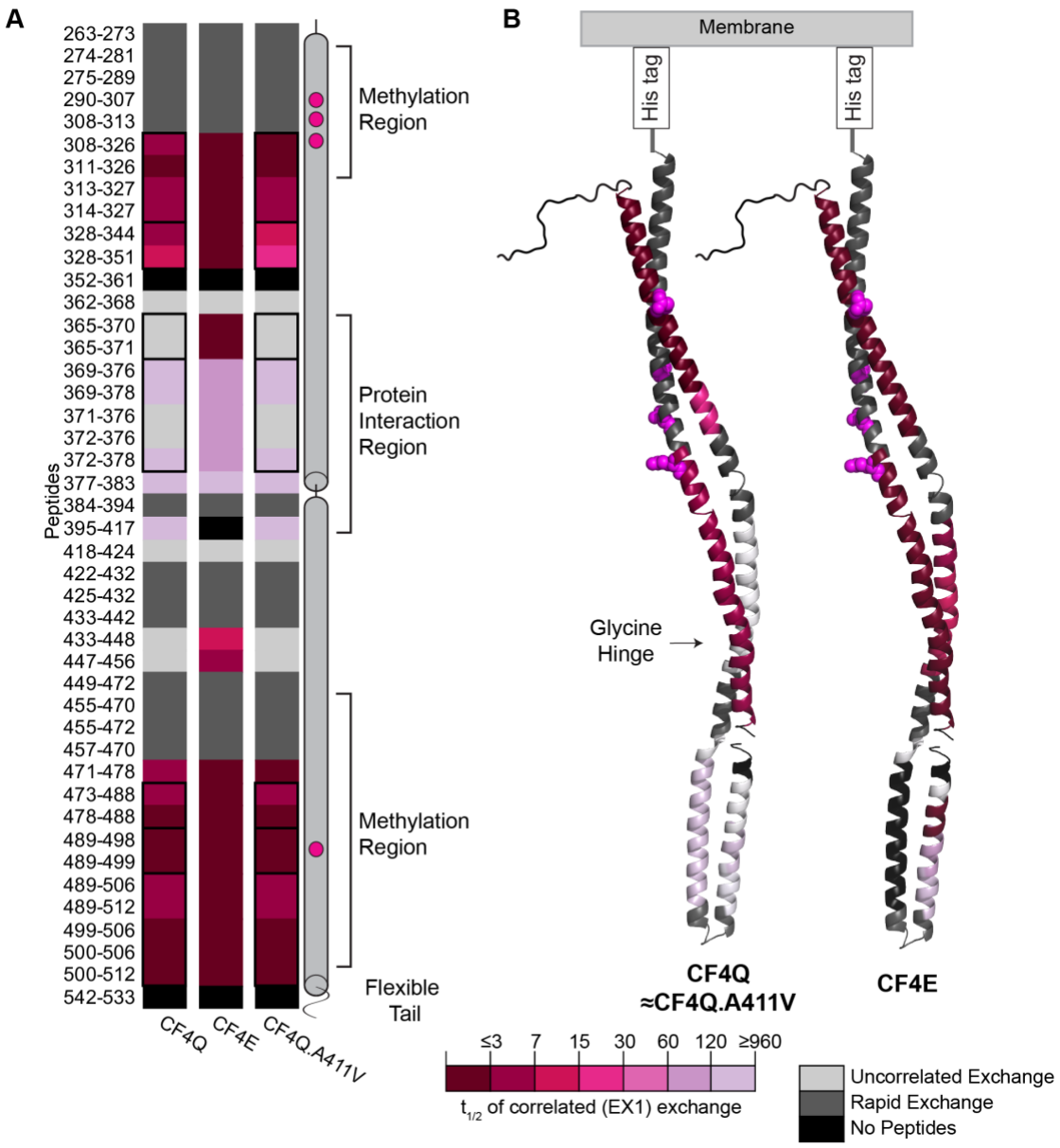

Figure 3.9. Estimated $t_{1/2}$ of correlated exchange (EX1) of peptides throughout CF in functional complexes with CheA and CheW. (A) The $t_{1/2}$ for correlated HDX of peptides in each of the three states is represented by a color scale, from dark maroon to pale purple for fast to slow correlated HDX (short to long $t_{½}$), with light gray representing peptides with uncorrelated exchange. When exchange is rapid (peptides represented in dark gray with > 70% exchanged in 3 min), it is difficult to detect correlated HDX. (B) CF monomer structure (from pdb file 1qu7) is colored according to the estimated EX1 $t_{1/2}$ for CF4Q (left, which is very similar to the profile for CF4Q.A411V) and CF4E (right). Methylation sites are labelled in magenta in both A and B.

The emerging picture is that CF within functional complexes in all three states exhibits widespread correlated exchange throughout its structure. EX1 HDX processes are observed in all regions shown in maroon to pale purple, and may also occur in regions shown in dark gray, where it cannot be detected due to the time resolution of the experiments. This suggests the entire CF populates a long-lived unfolded state. Furthermore, the top 2/3 of the CF in these complexes shows rapid exchange, either >70% exchange within 3 min (correlated or uncorrelated, dark gray in Fig 3.9B), or correlated exchange with a short $t_{1/2}$ of 3-15 min (dark maroon to red in Fig 3.9B). In contrast, the protein interaction region where CF binds to CheA and CheW shows significantly slower exchange, with longer estimated $t_{1/2}$ values of 120 min to >960 min. This is consistent with the deuterium uptake analysis discussed above, suggesting that protein interactions stabilize the CF in this region.

The changes in correlated exchange between CF4Q and CF4E are highlighted in Figure 3.10. The stacked spectra in Figure 3.10A illustrate the changing values of $t_{1/2}$ for these two states, and these changes are represented by colors on the CF monomer structure in Figure 3.10B. Peptides 371–376 and 377–383 exhibit a reduction in $t_{1/2}$ from CF4Q to CF4E (960 to 120 min, and >960 to 960 min, respectively). These peptides represent the 369-383 region that exhibits protection from complete exchange at long times due to protein interactions (see Figure 3.3-3.4), suggesting a "loosening" of the stabilizing protein interactions in CF4E. Peptides 365-370 and 433-448 exhibit a change from uncorrelated exchange in CF4Q to correlated exchange with $t_{1/2}$ of 3-15 min in CF4E. Looking back at Figure 3.9B, this corresponds to an expansion of the region with rapid correlated exchange

(dark maroon to red) or >70% exchange in 3 min (dark gray) to the entire structure of CF4E, other than the protein interaction sites.

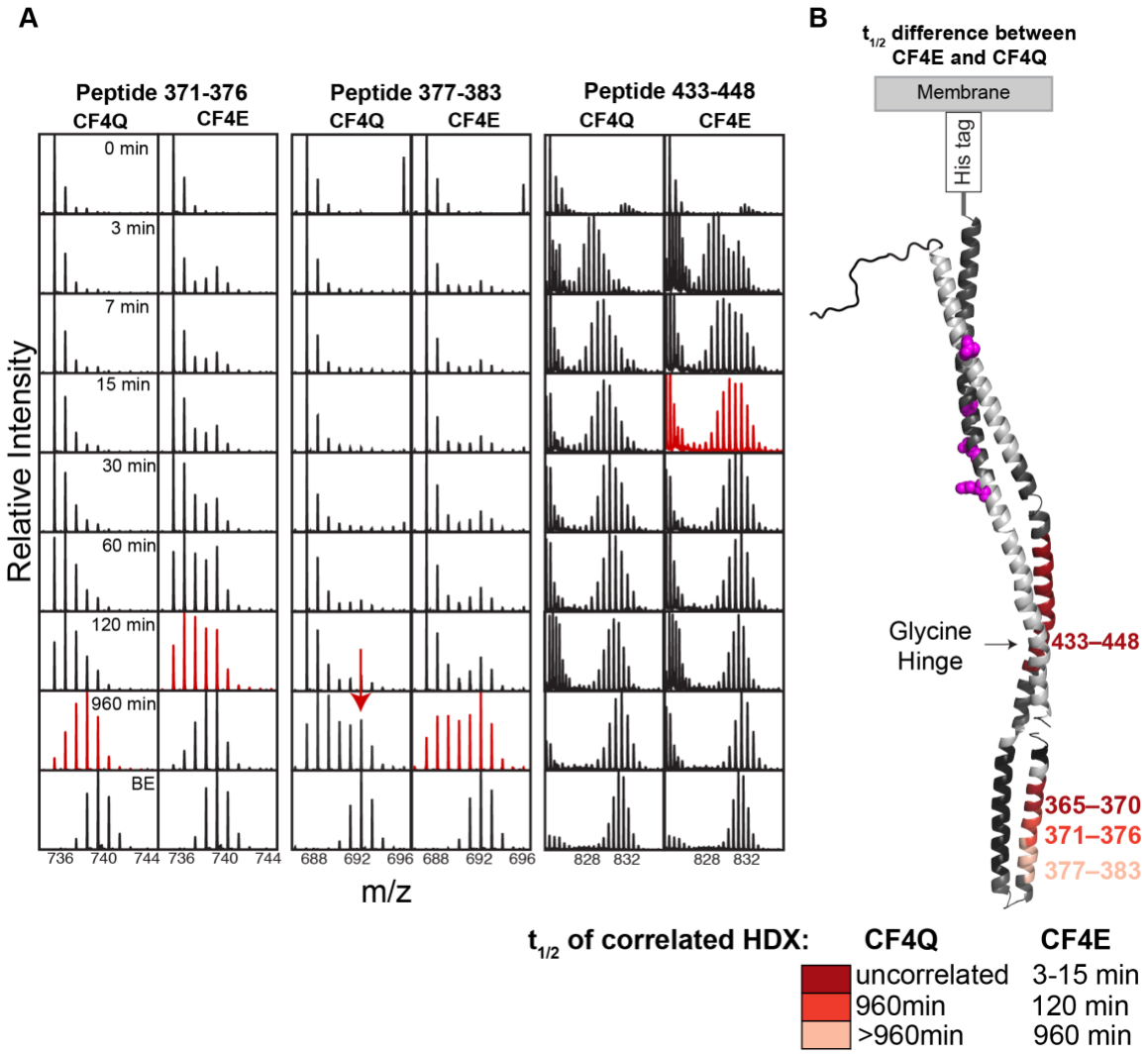

Figure 3.10. Regions with differences in $t_{1/2}$ of correlated HDX between CF4Q and CF4E. (A) Stacked plots of mass spectra *vs* HDX time for representative peptides illustrate $t_{1/2}$ differences (BE is back exchanged sample). Red arrow indicates $t_{1/2}$ of peptides is more than 960 min. (B) Differences in $t_{1/2}$ of correlated exchange are represented by colors on CF monomer structure. As in previous figures, black indicates no peptides observed, dark gray indicates very fast exchange (>70% exchange within 3 min), and light gray indicates uncorrelated HDX or no change in $t_{1/2}$ of correlated HDX.

Finally, overlays of the mass spectra for CF4Q and CF4E illustrate that a number of peptides show a change in rates of both correlated and uncorrelated exchange. This is

illustrated for peptide 314–327 by an overlay of 3 min spectra in Figure 3.11: for green (CF4Q) to orange (CF4E), the shift to higher m/z of the mass envelope with partial exchange indicates a shift to faster uncorrelated exchange (black arrows, ΔEX2); the shift to a larger mass envelope with complete exchange indicates a shift to faster correlated exchange (red arrows, ΔEX1). Similar behavior is observed for many peptides, including 308-327, 313-327, 314-327, 328-351, 471-478, 473-488, 489-506, 500-512. This corresponds to all regions with rapid correlated exchange (dark red colors in Figure 3.9).

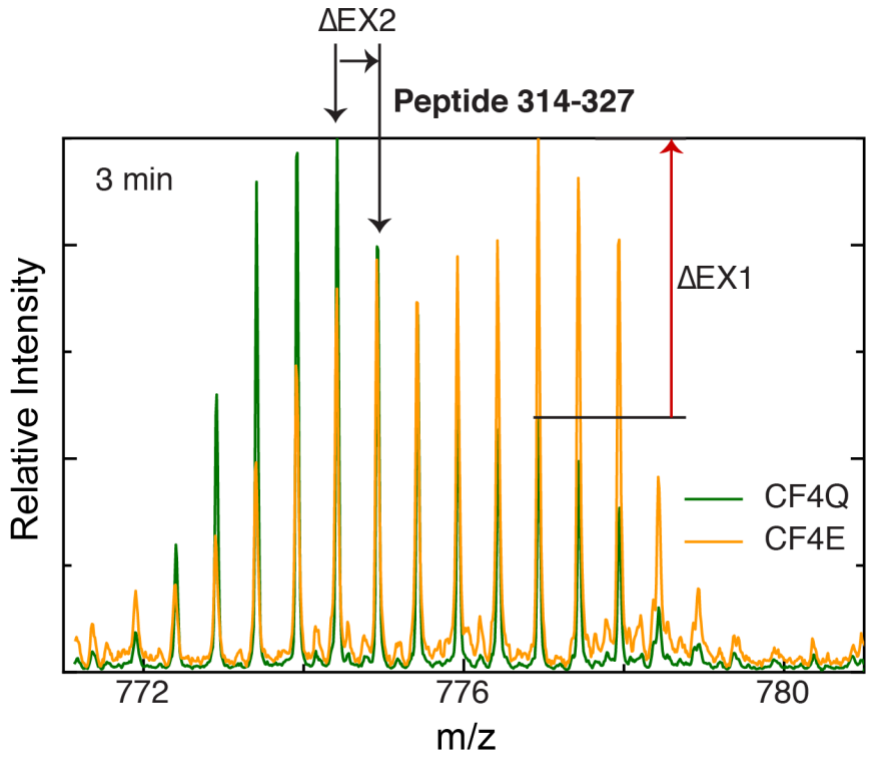

Figure 3.11. Overlaid spectra show changes in rates of both correlated (EX1) and uncorrelated (EX2) exchange. Differences in mass spectra of peptide 314–327 after 3 min HDX demonstrate that CF4Q (dark green) exhibits both slower EX2 (judged by m/z position of mass envelope, black arrows) and slower EX1 (judged by intensity of mass envelope, red arrows) relative to CF4E (orange).

CHAPTER 4

HDX-MS RESULTS ON FUNCTIONAL SIGNALING COMPLEXES: PRELIMINARY OVERVIEW OF DYNAMICS OF THE KINASE CHEA

4.1. Introduction

Understanding signaling requires understanding how the receptor controls the kinase activity of CheA. CheA consists of five domains: P1(residues 1-134) contains the His residue that is phosphorylated; a flexible linker (135-158) connects P1 to P2; P2 (159-229) is the docking site for CheY and CheB that facilitates phosphotransfer to these proteins; another linker (230-260) connects P2 to P3; P3 (261-325) is the dimerization domain; P4 (326-507) contains the ATP binding site; and P5 (508-654) binds to the receptor and CheW (Mo et al., 2012) (Figure 4.1). To complement the results presented in Chapter 3, HDX-MS can be used to investigate how CheA domains change their structure and dynamics to control the kinase activity and build a more complete picture of the mechanism of signaling transduction.

Recent electron cryotomography (ECT) and molecular dynamics studies suggest that dynamics of CheA domains may play a role in the control of kinase activity. ECT of intact receptor mutants revealed that the CheA P1-P2 domains show less density in the kinase-on state, suggesting greater mobility of these domains. It was proposed that the kinase is activated when P1 is released for productive interactions with the catalytic P4 domain (Briegel et al., 2013). In another study, molecular dynamics simulations revealed a “dipping” motion of the CheA-P4 domain, which is proposed to be involved in control of kinase activity (Cassidy et al., 2015). The HDX-MS approach we have implemented to measure changes in receptor dynamics within functional complexes is ideally suited for detection of changes in CheA dynamics to test these mechanistic proposals. Furthermore,

the results presented in Chapter 3 suggest a weakening of the interaction between the receptor and the CheA-P3 domain, based on the kinase-off state exhibiting reduced protection from exchange at long times at the P3 interaction site. This predicts complementary changes in CheA-P3, which can also be tested with the HDX-MS approach. Interestingly, the P4 'dipping' observed by MD simulations is accompanied by disruption of the receptor/P3 interaction (Cassidy et al., 2015), which is consistent with the faster HDX we observed for the kinase-off state at the receptor/P3 interface .

Using HDX-MS to measure changes in structure and dynamics of CheA requires samples that are homogeneous with respect to CheA, with all of the CheA incorporated into functional arrays with CF and CheW. The HDX experiments reported in Chapter 3 were performed on samples optimized for the homogeneity of CF, with excess CheA and CheW present to drive all of the CF into functional complexes. Although these samples are not ideal for monitoring CheA dynamics, because they contain a mixture of bound and free CheA, the experiments yielded data on HDX of CheA that can be analyzed to test the feasibility of an HDX-MS study of CheA.

As reported in Chapter 3, 183 CheA peptides were identified in the HDX-MS studies on native-like functional arrays of CF, CheA, and CheW bound to vesicles. As shown in Figure 4.1, this corresponds to 69% sequence coverage of CheA, with peptides identified from all the CheA domains and linkers. Table 3.1 indicates that about 4 μM CheA was incorporated into the functional complexes, leaving 8 μM free CheA. Thus HDX-MS of these samples will reflect the properties of both free CheA (2/3) and bound CheA (1/3).

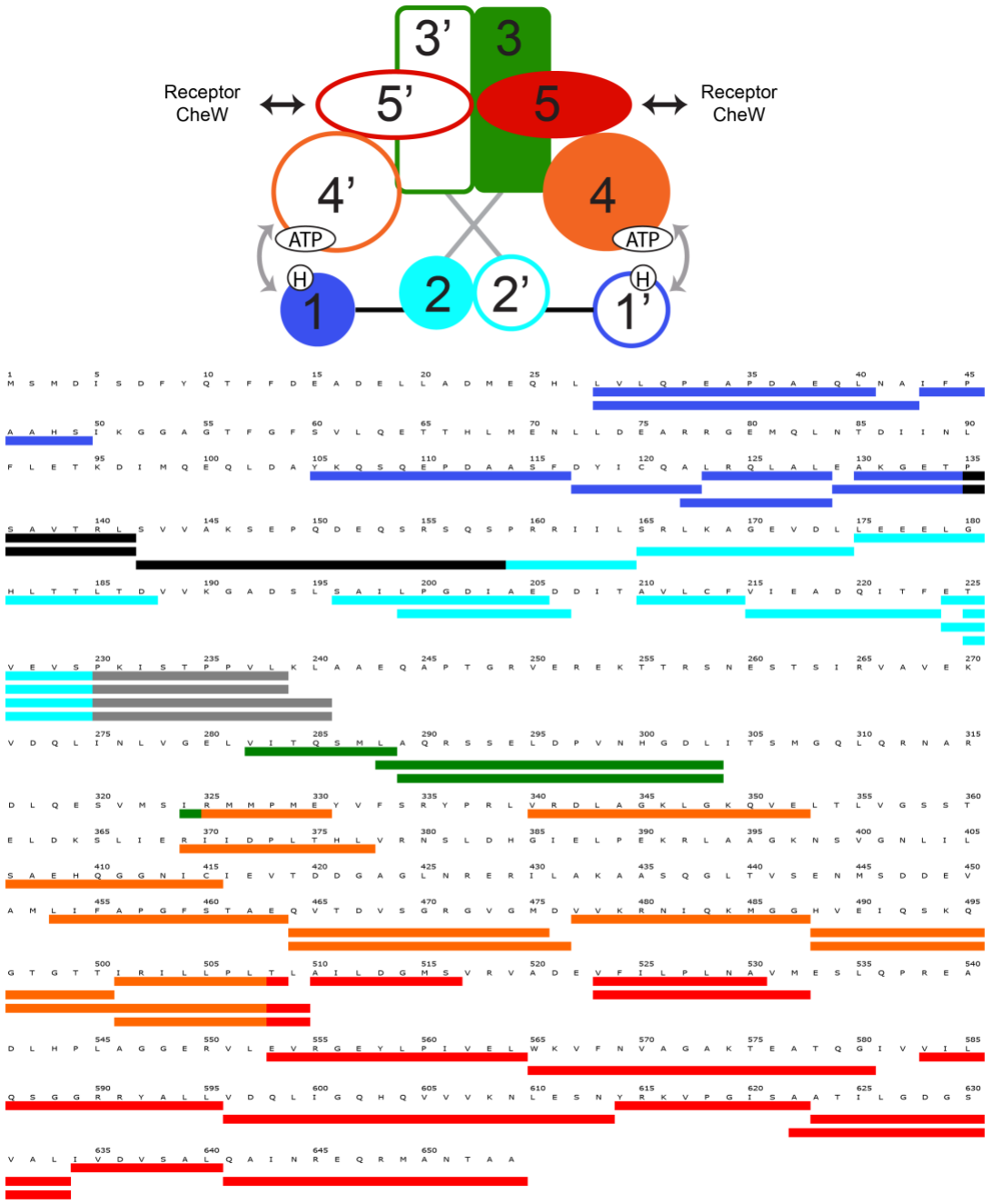

Figure 4.1. HDX-MS identifies peptides from all domains and linkers of CheA. (A) Cartoon of CheA domains and interactions, and (B) CheA sequence and peptides identified in the HDX-MS experiment (69% coverage), with each domain represented in different colors, and the linkers represented in black and gray.

4.2. Developing a protocol to prepare a fully exchanged CheA control sample

Since CheA is a large multidomain protein, it is unlikely that heat denaturation of CheA is reversible. Therefore, we sought to use cycles of lyophilization/resuspension in D_2O buffer to prepare a fully exchanged CheA sample. The first step was to determine whether CheA could retain activity following such a procedure. For lyophilization, a 100 µL aliquot of 264 µM CheA in kinase buffer was placed in an Eppendorf tube. The cap was removed and replaced with parafilm, with tiny holes in the parafilm for removal of fluid during lyophilization. CheA was flash frozen with liquid nitrogen, the frozen Eppendorf tube was placed in the 300 mL fast-freeze flask (Labconco), connected to the lyophilizer (Labconco lyophilizer in Thai lab), and then left under vacuum overnight at 0.31mBar and -103°C. The CheA lyophilized powder was then resuspended to the original volume in 1X D_2O kinase buffer. Some of this sample was retained and some was subjected to a second lyophilization and resuspension. Both 1x and 2x lyophilized CheA samples were tested for kinase activity: PEG complexes containing 50 µM CF4Q, 12 µM CheA, 20 µM CheW, 4% (w/v) PEG 8000, 4% (w/v) D-(+)-trehalose, and 1mM PMSF in kinase buffer were incubated overnight in a 25°C water bath, and kinase activity was measured the next day. The results shown in Figure 4.2 indicate that CheA retains kinase activity after two rounds of lyophilization/resuspension, and lyophilization can be used to prepare a fully exchanged CheA control for HDX-MS experiments. The MS sample was made by diluting the D_2O exchanged CheA to 12 µM using 1x D_2O kinase buffer, adding 22.5 µL of this CheA to a prechilled Eppendorf tube that contained 22.5 µL cold quench buffer, flash freezing immediately with liquid nitrogen, and storing at -80°C. HDX samples of free

CheA were prepared using a G10 sephadex zeba desalting column (Pierce Biotechnology) as described in Chapter 2.

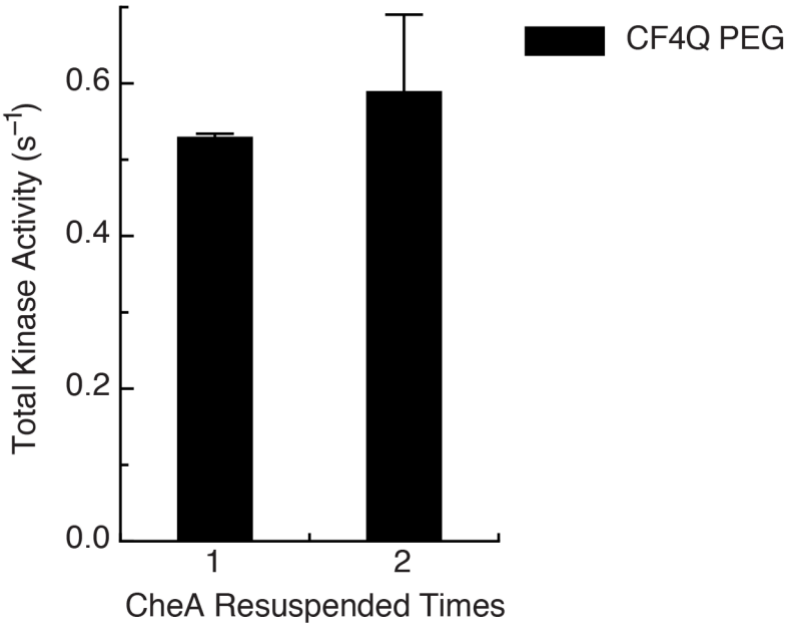

Figure 4.2. Effect of lyophilization on kinase activity of CheA. CF4Q PEG complexes are assembled using 50 µM CF4Q, 12 µM CheA and 20 µM CheW, 4% (w/v) PEG 8000, 4% (w/v) D-(+)-trehalose. These samples incorporated CheA that had been lyophilized 1x, or 2x. Total kinase activity is based on the full amount of CheA in the sample and is within the range of activity levels typically observed for PEG-mediated complexes of CF4Q. Activities are average of three replicates measured on the same day.

Unfortunately, the fully exchanged CheA control showed less deuterium uptake than other time points. This indicates that the CheA was not fully exchanged, suggesting there was too little time in the D_2O kinase buffer for complete exchange before lyophilization. In the future, leaving CheA at 25°C for 30 min after resuspending the lyophilized CheA in 1x D_2O kinase buffer should increase the level of exchange in this control sample.

4.3. Preliminary comparison of HDX of free CheA *vs* CheA incorporated into kinase-on and kinase-off complexes

HDX-MS data for free CheA, CheA in kinase-on complexes, and CheA in kinase-off complexes were analyzed in one DynamX file, giving a CheA peptide coverage of 46% and redundancy of 1.37 (Figure 4.3). Analyzing all three states of CheA in one DynamX file is a good approach for a rapid preliminary analysis, because the software can quickly generate a heat map comparing deuterium uptake of all CheA peptides in the three states. However, it greatly reduced the CheA peptide coverage because peptides must be present in all three states in order to be included in the analysis. Separate analysis of each state of CheA state gives higher coverage (eg 69% shown in Figure 4.1). The colors in Figure 4.3 (same colors as in Figure 4.1) show that despite the reduced coverage, peptides from all domains and linkers are observed.

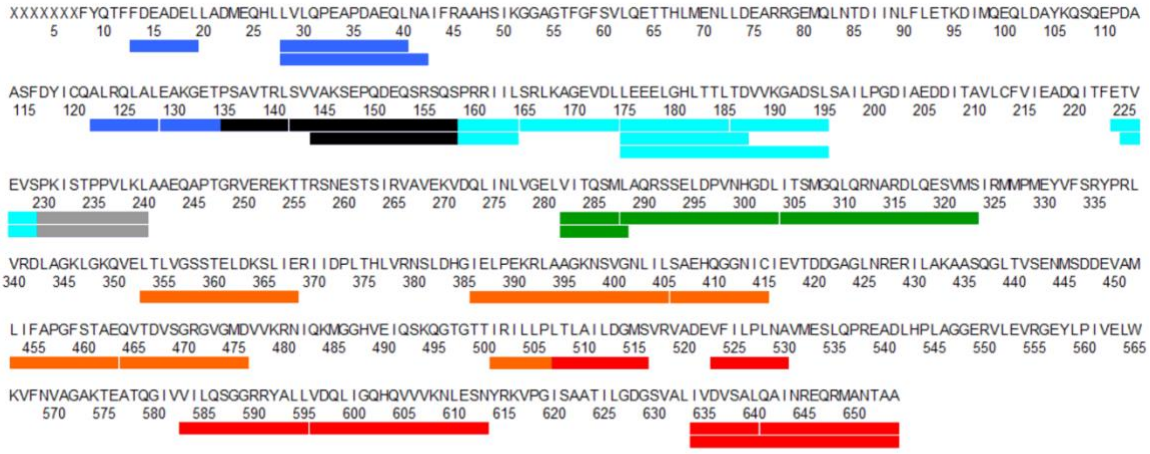

Figure 4.3. Peptides observed in HDX-MS of all three states of CheA (kinase-on, kinase-off and free CheA). This rapid analysis yields only 31 peptides, 46% CheA peptide coverage and 1.4 redundancy. CheA sequence is shown on the top, bars represent individual CheA peptides with colors corresponding to the different domains of CheA in Figure 4.1.

Figure 4.4 compares the heat map of CheA peptide HDX in kinase-on complexes (top row), kinase-off complexes (middle row) and free CheA (bottom row). Each row shows colors representing the percent deuterium uptake at 3 min, 15 min and 16 hr time points. For these data, uptake is expressed as a percentage of each peptide's maximum possible uptake (in contrast to the CF data in chapter 3 that was expressed as a percentage of the fully exchanged control). Percent uptake is represented in rainbow colors from blue to red indicating low to high deuterium incorporation.

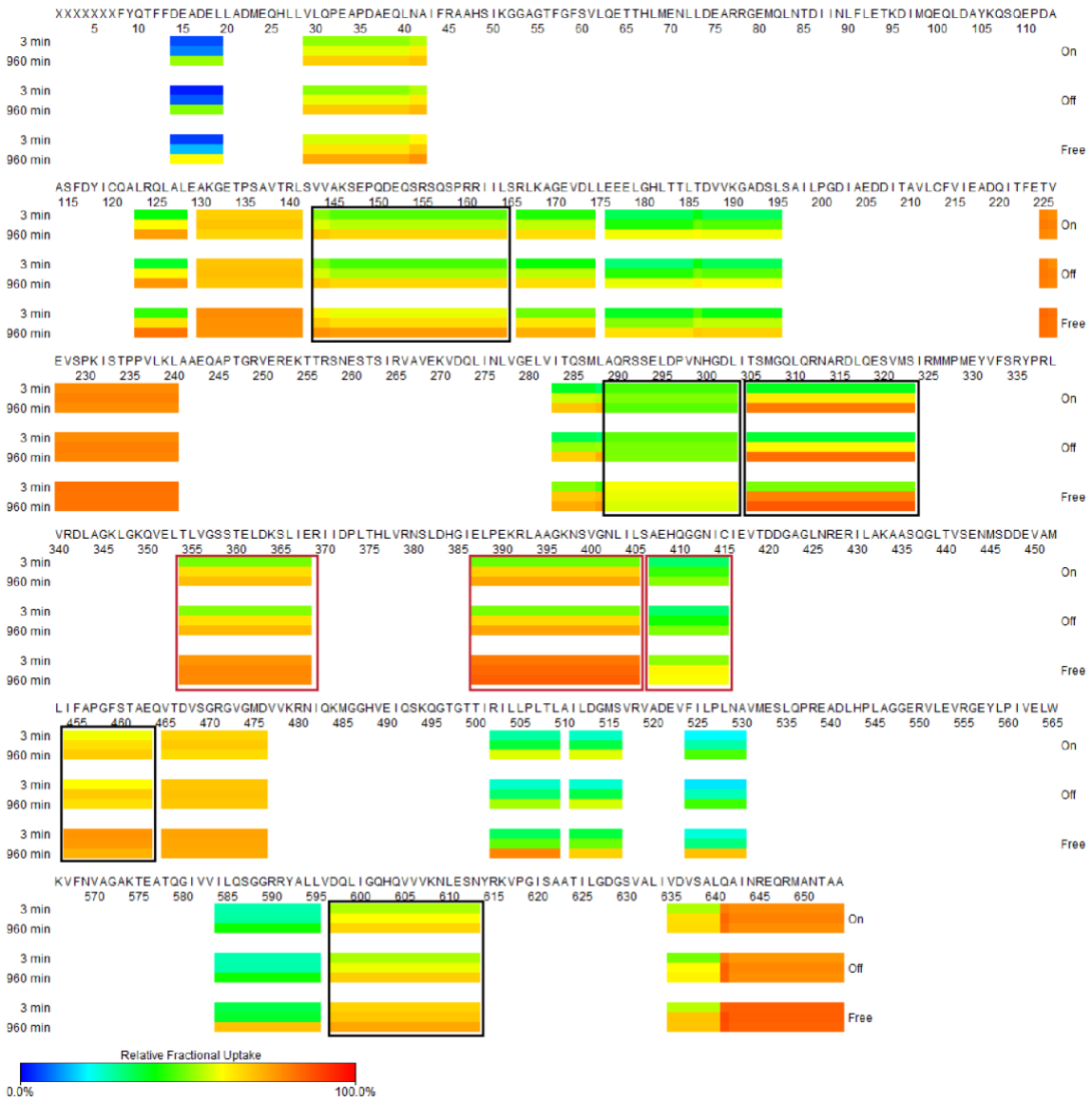

Figure 4.4. CheA heat map comparing HDX time course for kinase-on and kinase-off complexes with free CheA. Percent deuterium uptake (expressed as a percentage of each peptide's maximum possible uptake) at each time point is represented in rainbow colors from blue to red indicating low to high deuterium incorporation. Uptake differences are observed between free CheA (bottom rows) and CheA in complexes (top and middle rows). Differences are highlighted with boxes: black boxes represent differences >10% and red boxes represent differences ≥20%.

The heat maps for the kinase-on and kinase-off complexes are very similar, but somewhat different from free CheA. Heat maps for peptides that show differences in uptake between complexes and free CheA are enclosed by boxes: black boxes indicate >10% difference; red boxes indicate >20% differences. Small differences (>10%) are observed in the P1-P2 linker through the beginning of the P2 domain, as well as the P3, P4 and P5 domains. Larger differences (>20%) are observed only in the P4 domain. However, with only a single replicate for the free CheA sample, we can't tell whether or not the difference has exceeded the significance level. The peptides from CheA in complexes show less deuterium uptake than free CheA, which suggests that HDX is detecting increased domain-domain and protein-protein interactions in the active complexes that reduce the solvent exposure compared to free CheA. Comparisons of HDX of intact CheA, CheA domains, and CheA in complexes may be useful to deduce the domain-domain and protein-protein contacts of CheA that are present within functional complexes.

No significant difference in deuterium uptake of CheA was observed between kinase-on and kinase-off complexes. This may be due to the fact that only 1/3 of CheA in the sample is incorporated into functional complexes, and the HDX behavior is skewed towards the properties of free CheA. Despite this limitation, observation of some differences between CheA in complexes and free CheA suggests that an HDX-MS study on samples optimized for full incorporation of CheA into complexes would yield

information on CheA domain interactions and mobilities to provide insights into the mechanism of control of kinase activity.

CHAPTER 5

INSIGHTS INTO THE SIGNALING MECHANISM

5.1. Implications of HDX behavior regarding the properties of CF

Hydrogen exchange of the CF in functional complexes with CheA and CheW ranges from very fast near the N and C termini, to fast throughout most of the CF, to very slow at the protein interactions sites near the membrane-distal cytoplasmic tip (Figure 3.3 & 3.4). Very fast exchange (complete within 3 min) is observed from the N-terminus through the N-terminal side of the methylation region. This segment includes part of the HAMP domain, and its connection to the methylation region with a helix stutter that creates an inverse stability relationship between the HAMP helices and the N-terminal methylation helix (Zhou et al., 2009). Similarly, fast exchange is observed for the C-terminal tail that is thought to function as a flexible tether to the CheR binding site at the C terminus of the receptor, suggesting that both these N and C-terminal regions are unstructured. At the other extreme, the protein interaction region shows very slow exchange, which is not complete at 16 hr due to interactions with its binding partners CheA and CheW. This remarkable range of HDX rates reflects the dual nature of the CF, from the disordered regions of the HAMP-methylation segment and C-terminal tail to the highly ordered membrane-distal region that packs with CheA and CheW into an extended hexagonal lattice.

The other notable aspect of the HDX results is that the CF exhibits widespread correlated exchange (EX1) (Fig 3.9), and t½ values are short everywhere except the sites of protein interactions with CheA and CheW. This suggests the entire CF populates a long-lived unfolded state, and binding of CheA and CheW induces folding. Consistent with this

picture, all regions of CF other than these protein interaction sites exhibit fast exchange (>50% in 15 min).

5.2. How do these results compare with previous studies of CF dynamics?

The current HDX study has made significant improvements over a previous HDX study (Koshy et al., 2014) in both the samples and the MS data. The samples used previously were similar, but CF4E complexes were assembled at low density (high vesicle surface area, kinase-off state) and high density (low vesicle surface area, kinase-on state). We have since realized that the high density conditions did not have sufficient vesicle surface area to allow all of the CF to assemble into functional complexes with CheA and CheW. We estimate that the limited vesicle surface area of the high density samples led to 47% of the CF4E being bound within close-packed CF-only regions rather than forming the hexagonal array with CheA and CheW. As observed in the current study, Koshy *et al* observed incomplete exchange at 16 hours, with a similar number of protected sites in the low density homogeneous samples, but a ~two-fold larger number of protected sites in the high density inhomogeneous samples. It seems likely that this larger protection is a property of the close-packed CF of this heterogeneous sample, and could also be due to decreased solvent exposure under the high density assembly conditions. Thus, the use of a mutant to control signaling state for the current study is an improvement over the use of packing density by Koshy et al, because the latter could change HDX by changing solvent exposure. By assembling the complexes at the same density in this study (with sufficient vesicle surface area for all of the CF to assemble into functional complexes with CheA and CheW), any difference in HDX we observe is not due to an effect of their density of binding

to the vesicle surface, and can be more confidently assigned to the change in signaling state.

The current study also makes improvements in the mass spectrometry. We used a Water Synapt G2Si with ion mobility separation to identify peptides, leading to better reproducibility and resolution. Shorter and more peptides allow us to better localize the protection and see that it matches the CheA and CheW binding sites. Overall, the results of both HDX studies are consistent. Both the current and previous study (Koshy et al., 2014) observed (1) very rapid exchange near the N and C termini, (2) protection from complete exchange near the membrane-distal tip, (3) a kinase-on state with slower exchange in the methylation region and greater protection in the protein interaction region, and (3) mass spectra with evidence of correlated exchange.

Our HDX results are also consistent with dynamics observed by other methods. One EPR study examined site-specific spin labels to measure the mobility of helices of the cytoplasmic domain of intact Tar inserted into nanodiscs, but lacking CheA and CheW (Bartelli and Hazelbauer, 2016). Consistent with our results, they observed that the N-helix is more dynamic than the C-helix, and the methylation region is more dynamic in the unmethylated state. However, they saw no effect of ligand binding on the dynamics, which may be due to the absence of CheA and CheW. It has been demonstrated that full coupling between ligand binding and the cytoplasmic domain (eg methylation effects on ligand affinity) is only observed in ternary complexes of the receptor, CheA, and CheW (Li and Weis, 2000). Another EPR study examined site-specific spin labels incorporated into kinase-on and kinase-off fusion constructs containing the Tar methylation and protein interaction domains linked to variants of the Aer HAMP domain, but again in the absence

of CheA and CheW (Samanta et al., 2015). In these samples, the HAMP domain shows increased dynamics in the kinase-on state and, consistent with our results, the protein interaction region shows decreased dynamics in the kinase-on state. Finally, a recent solid-state NMR study (Kashefi and Thompson, 2017) on functional CF complexes assembled with CheA and CheW on vesicles (equivalent to samples used in this study) reports that the N-terminal methylation helix is dynamic on the ns timescale, and these dynamics increase in the kinase-off state. All of these results using different methods and samples are consistent with our current HDX results on the following points: the N-terminal methylation helix is highly dynamic, the methylation region dynamics are reduced in the methylated state, and the protein interaction region dynamics are reduced in the kinase-on state.

5.3. Insights into protein interactions between CF, CheA, and CheW

As shown in Figure 3.3, the incomplete exchange at 16 hr appears to be at the binding interfaces in the functional complex. Looking more closely, it is clear that the protected peptides are consistent with other published observations of these binding interfaces, as illustrated in Table 5.1. These studies include solution NMR transverse relaxation optimized spectroscopy (TROSY) studies on a truncated version of a soluble chemoreceptor to identify receptor residues that undergo chemical shift changes upon binding CheA or CheW (Wang et al., 2012b) (Vu et al., 2012). Most of the residues identified in these studies are found within the peptides that show incomplete HDX; the exceptions are shown in red in Table 5.1. Note that the NMR studies used a P4-P5 construct of CheA, and thus did not detect the receptor/P3 interaction that we have detected with HDX. Another study used in vivo cross-linking to detect the interaction between Tsr and

CheW proteins, and showed that Tsr V388C and R398C form crosslinks with CheW, but the presence of CheA decreased the cross-linking efficiency for Tsr V398C and increased the cross-linking efficiency for Tsr R388C (Pedetta et al., 2014). These two receptor residues are listed in red in Table 5.1 because they are not found within the peptides that show incomplete HDX; this may be because Cys disulfide formation probes longer-range contacts. Finally, there are two current models for the receptor array: (1) the Crane model based on an x-ray crystal structure of a CF/CheA/CheW complex (3ur1) and ECT studies of intact receptors in cells (Briegel et al., 2012), and (2) the Cassidy model based on ECT studies of CF complexes assembled on lipid monolayers and MD simulations (Cassidy et al., 2015). Analysis of these models to identify receptor residues within 3 Å of CheA or CheW yields the residues listed in Table 5.2. Again, most of these residues lie within the peptides with incomplete HDX. Note that some of the experimental data listed in Table 5.1 was obtained from nonfunctional complexes. The experiments on functional complexes (highlighted in green) are the ECT of arrays in cells (Briegel et al., 2012), ECT of CF arrays bound to lipid monolayers (Cassidy et al., 2015), disulfide crosslinking of complexes in cells (Pedetta et al., 2014), and HDX of CF arrays bound to lipid vesicles (this study).

Table 5.1. Receptor residues interacting with CheA and CheW.

Protein Interaction (proteins present)[a]	Method (reference)	Receptor Residues Involved in Interaction[b]
Receptor/CheA (TM0014$_{90\text{-}206}$[c] CheAΔ354[d])	NMR[h] (Wang et al., 2012a)	375, 376, 378, 382
Receptor/CheA (Tm14s[e] CheAΔ354[d] CheW) for X-ray, in vivo for EM	X-ray (3UR1)/ECT model[i] (Briegel et al., 2012)	371, 375, 378, 379, 382, 386, 400, 406, 410

Receptor/CheA (Tar-CF, CheA, CheW)[f]	ECT/MD (3JA6)[i] (Cassidy et al., 2015)	369, 375, 378, 379, 392
Receptor/CheA (Tar-CF, CheA, CheW)[g]	HDX-MS[j] (this study)	372-383, 395-417
Receptor/CheW (TM0014$_{90-206}$[c] CheW)	NMR[h] (Wang et al., 2012a)	375, 376, 378, 382
Receptor/CheW (TM0014$_{90-206}$[c] CheW)	NMR[k] (Vu et al., 2012)	372, 377, 379, 380–383, 385, 386, 396
Receptor/CheW (Tsr, CheA, CheW)	In vivo cross-linking of Cys mutants (Pedetta et al., 2014)	386, 396
Receptor/CheW (Tm14s[e] CheAΔ354[d] CheW), in vivo for EM	X-ray crystallography (3UR1)/ECT model[l] (Briegel et al., 2012)	378, 379, 381, 383
Receptor/CheW (Tar-CF, CheA, CheW)	ECT/MD (3JA6)[l] (Cassidy et al., 2015)	375, 378, 379, 382, 383, 385, 386, 392, 402
Receptor/CheW (Tar-CF, CheA, CheW)	HDX-MS[j] (this study)	372-383

[a]Only the protein complexes highlighted in green are functional

[b]Asp receptor (*E. coli* Tar) residue numbers are obtained as follows: TM0014 number + 240 = Tar number; Tm14s number - 2002 = Tar number; Tsr number - 2 = Tar number. Red indicates contacts reported in previous studies that are not within the regions with incomplete HDX at 16 hr.

[c]TM0014$_{90-206}$ is a truncated version of TM0014, a single chain soluble chemoreceptor which lacks the transmembrane region and does not support trimer-of-dimer formation (Vu et al., 2012).

[d]CheAΔ354 is a monomeric construct containing only P4 and P5

[e]Residues 107-191 of the *T maritima* receptor Tm14s, corresponding to the protein interaction domain.

[f]Functional complexes assembled on lipid monolayers.

[g]Functional complexes assembled on lipid vesicles.

[h]Chemical shift perturbation of receptor ^{13}C-methyl ILV sidechains upon binding

[i]Residues of Tar that are within 3Å of CheA in Crane model or 3JA6.

[j]Incomplete HDX at 16 hr.

[k]Chemical shift perturbation of receptor ^{15}N-amide backbone upon binding

[l]Residues of Tar that are within 3Å of CheW in Crane model or 3JA6.

Table 5.2 lists numbers of remaining protons at 16 hr in the peptides of the protein interaction region that exhibit incomplete exchange. Protection levels were determined by subtracting the mass at 16 hr from the mass of the fully exchanged control (which corrects for back exchange). The peptides of the membrane-distal cytoplasmic tip are listed in Table 5.2; these show a range of 0.9–4.4 Da unexchanged at 16 hours, except peptide 384-394 which exhibits complete HDX. Bold red text in this table highlights significant (≥ 0.9 Da) changes in the residual protons: 4Q *vs* 4E exhibit a change in the 369-378 range and kinase-on *vs* kinase-off exhibit a change in the 395-417 range.

Table 5.2. Number of protons remaining after 16 hr of HDX in functional complexes of CF4Q, CF4E and CF4Q.A411V.[a]

	Peptides	CF4Q (Da)	CF4E (Da)	CF4Q.A411V (Da)
1	369-376	**1.66±0.8**	**0.76±0.04**	0.93±0.07
2	369-378	**2.96±0.3**	**1.54***	2.22*
3	371-376	1.59±0.3	0.78±0	1.16*
4	372-376	1.29*	0.74*	1.01*
5	372-378	**2.35±0.3**	**1.3±0.07**	1.77±0.2
6	377-383	2.58±0.04	1.96±0.2	3.03±0.03
7	377-393	--	2.69*	3.86*
8	379-393	--	1.68*	--
9	379-394	--	--	3.14±0.4
10	381-393	--	--	1.21*
11	384-394	Complete exchange	Complete exchange	Complete exchange
12	394-417	--	2.11*	--
13	395-414	--	1.25*	--
14	395-417	**4.4±0.7**	--	**2.78±0.4**
15	401-417	--	1.46±0.1	1.76±0.3

[a]Numbers of unexchanged protons are the average ± standard deviation of two replicates, except where an asterisk indicates a single observation of that state. No data (--) indicates the peptide was not observed in either replicate for that state. Significant differences (> 0.9 Da) between methylation states (CF4Q vs CF4E) or signaling states (CF4Q vs CF4Q.A411V) are highlighted in bold red text.

As shown in Table 5.3, the overlapping peptides listed in Table 5.2 can be used to further localize protected residues, which are likely to be at the protein-protein interaction sites. Such an approach on functional complexes may provide new insights for these and other important multi-protein complexes.

Table 5.3. Protected sites deduced from overlapping peptides with incomplete HDX.

Protected sites (subtracted peptides)[a]	CF4Q sites	CF4E sites	A411 V sites
369-370 (1-3)	0.07	-0.02	-0.23
371 (3-4)	0.3	0.04	0.15
372-376 (peptide 4)	1.29	0.74	1.01
377-378 (5-4)	1.06	0.56	0.76
377-378 (7-8)		1.01	
379-383 (6-(5-4))	1.52	1.4	2.27
381-383 (10-11)			1.21
394-400 (12-15)		0.65	
394 or 415-417 (12-13)		0.86	
395-400 (14-15)			1.02
401-417 (15)		1.46	1.76

[a]Numbers result from subtraction of the indicated peptides listed in Table 5.2.

5.4. HDX results lead to a new model for the signaling mechanism

The goal of our study was to compare the dynamic of the receptor in different signaling states and methylation states, both to test the proposed inverse dynamics model and to gain further insights into the signaling mechanism. The HDX results indicate that *both* the methylation region and protein interaction region of CF incorporated in functional complexes are stabilized in the kinase-on state relative to the kinase-off state (Figure 3.5), which is different from the proposed inverse dynamics model (Swain et al., 2009) in which the methylation region is stabilized but the protein interaction domain is *destabilized*.

Based on our HDX results we propose a new model for the signaling mechanism, illustrated in Figure 5.1, which involves modulation of an order/disorder transition of the receptor cytoplasmic domain. The CF apparently populates a long-lived unfolded state, based on the widespread correlated HDX. The correlated exchange is significantly slower at the protein interaction sites, suggesting that binding of CheA and CheW stabilize the CF. Free CF has been shown to be highly dynamic, with properties similar to a "molten globule." We propose that CF in arrays is less dynamic than free CF, but still populates a disordered state, and that signaling proceeds by modulating an order/disorder or folding/unfolding transition. Binding of CheA and CheW induces folding of CF, into a complex that activates the kinase (for simplicity, the model shown in Figure 5.1 shows only strong/weak binding of CheA, but similar changes may also apply to CheW). Demethylation and the ligand-induced piston each induce unfolding of CF, which in turn weakens the binding interactions with CheA and/or CheW, yielding a kinase-off state.

The observed slower HDX in both the methylation and protein interaction regions of the kinase-on state support this model, and also suggest that it is the interaction with

CheA-P3 that is weakened in the kinase-off state. However, the fact that greater HDX differences are observed with methylation state than with signaling state is not consistent with the model: the stabilization (HDX difference) is not proportional to the difference in kinase activity. There may be some explanation for this paradox: the A411V mutation may not faithfully represent the kinase-off state, or the crowded vesicle assembly may distort the properties of the demethylated state so that it does not faithfully represent a kinase-on state. Experiments are needed to test the predictions of the proposed model: (1) Do methylation and ligand-binding modulate the affinity of the receptor for CheA and CheW? (2) Does HDX of CheA-P3 reflect a decrease in its interaction with CF in the kinase-off state? (3) What HDX changes occur upon ligand binding to the intact receptor, the "true" kinase-off state? Modulation of a folding transition of the entire CF is an exciting new idea for explaining the integration of different inputs (ligand-induced piston and methylation) and the long-distance propagation of the signal 200Å from the membrane to the membrane-distal-tip of the receptor.

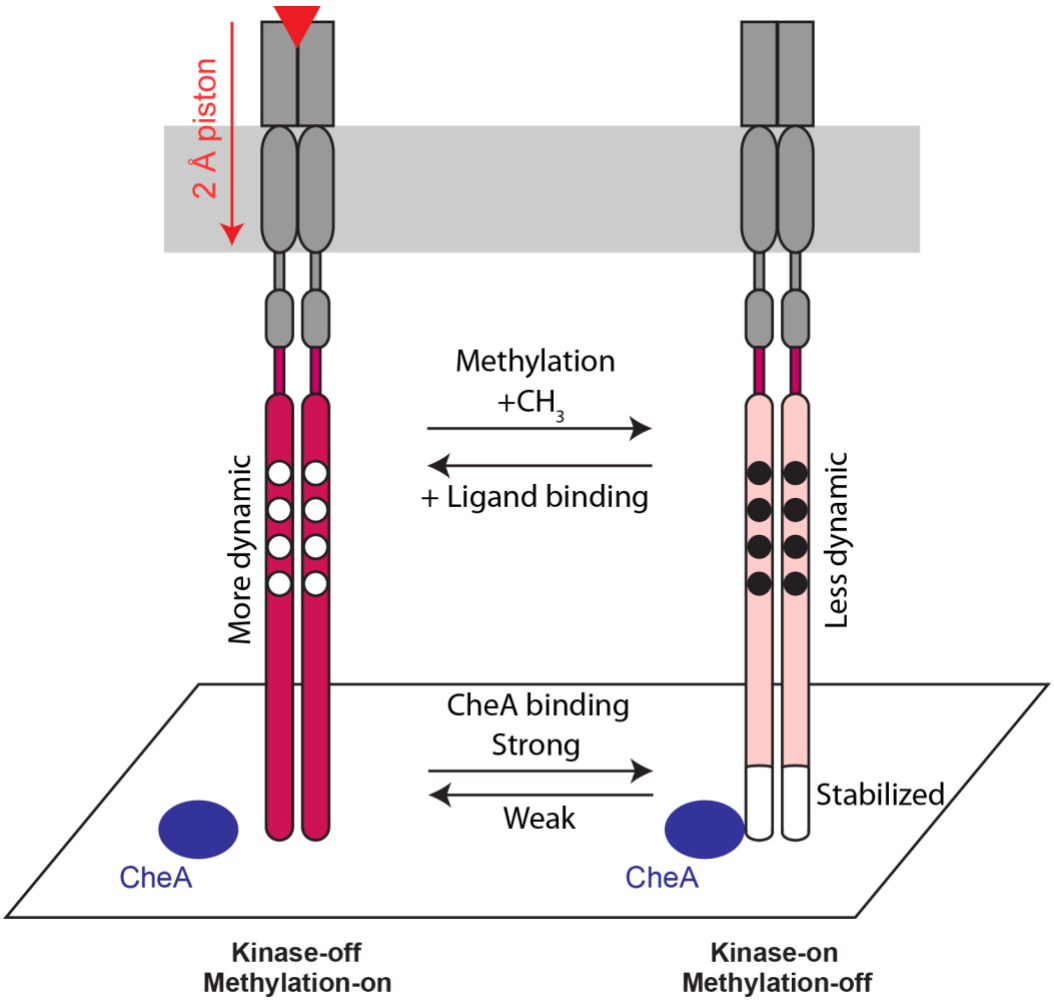

Figure 5.1. Proposed folding-mediated signaling mechanism. CF in arrays exhibits widespread correlated exchange, suggesting that CF populates a long-lived unfolded state. All regions except those interacting with CheA and CheW exhibit fast exchange, suggesting that only these protein interactions stabilize the unfolded state. We propose that CheA binds to CF in a kinase-on conformation and induces CF folding. Thus anything that destabilizes CF folding, such as the ligand-induced piston or demethylation, would weaken CheA binding and result in the kinase-off state. Note that CheA would not dissociate completely from the arrays, due to interactions with CheW.

APPENDIX

VESICLE SURFACE AREA FOR ASSEMBLY OF SIGNALING ARRAYS

The vesicle template assembly method was developed to assemble CF onto vesicles in functional complexes with CheA and CheW (Shrout et al., 2003). In this original study, a mixture of DOPC and DOGS-NTA-Ni^{2+} lipids was used to bind the His-tagged CF onto the vesicle surface, and substoichiometric amounts of CheA and CheW were included such that all of the CheA was incorporated into functional complexes. Our study instead aimed to use excess CheA and CheW to drive all of the CF into functional complexes. Thus it is important to estimate the vesicle surface area and choose a high enough lipid concentration for all of the His-tagged CF to bind to the vesicles and form hexagonal arrays with CheA and CheW. The vesicle surface area calculation below aims (1) to check what fraction of the His-tagged CF in the previous HDX study (Koshy et al., 2014) were in hexagonal arrays with CheA and CheW and (2) to demonstrate that the 725 μM lipid has sufficient surface area for assembly of all 30 μM His-tagged CF into functional hexagonal arrays.

In native cells, chemoreceptors form trimers-of-dimers that form hexagonal arrays with CheA and CheW. Three hexagons meet at each trimer-of-dimers, so each hexagon contains one dimer per vertex, for a total of 6 dimers per hexagon. The center-to-center distance between hexagons is 12 nm (Briegel et al., 2012). Figure A.1. illustrates the geometry of the hexagon and the fact that x is equal to 6 nm divided by cos 30°, so x = 6.93 nm.

To calculate the area of each hexagon: $3 \cdot \frac{\sqrt{3}}{2} \cdot (6.93\ nm)^2 = 124.7\ nm^2$

Area of each CF in hexagon: $$\frac{124.7\ nm^2}{6 \cdot 2\ CF} = 10.4\ nm^2\ per\ CF$$

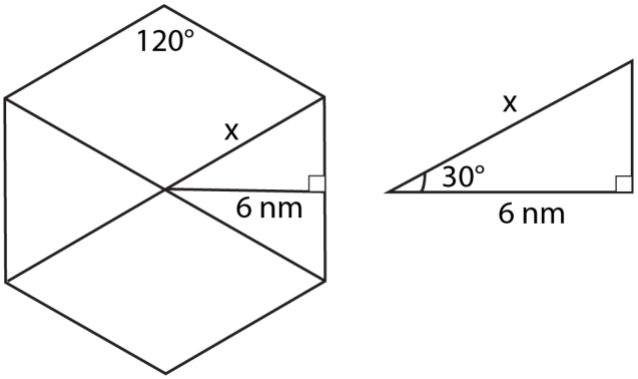

Figure A.1. Hexagon geometry in array. The center to edge distance is 6 nm, yielding a 12-nm center to center hexagonal spacing. Each internal angle is 120°, making x the hypotenuse of a 30-60-90 triangle.

A1. Fraction of CF in Koshy study that were in hexagonal arrays

In Koshy's study, CF functional complexes contained 30 μM CF and 580 μM total lipid which has 290 μM DOGS-NTA-Ni^{2+} and 290 μM DOPC. Calculation below shows the fraction of CF in Koshy's study in hexagonal arrays:

$$x+y=30\ \mu M$$

$$\frac{10.4\ nm^2}{CF} \cdot x + \frac{3.2\ nm^2}{CF} \cdot y = \frac{580\ \mu M\ total\ lipid}{2} \cdot 0.725\ nm^2$$

where x is the concentration of CF in hexagonal arrays with CheA and CheW; y is the concentration of CF bound close-packed to the vesicles; 0.725 nm^2 is the average membrane surface area of DOPC lipid per molecule (Nagle and Tristram-Nagle, 2000) and 3.2 nm is the area per non-array CF bound to vesicles (Besschetnova et al., 2008). Solving both equations yields x=15.87 μM, and 15.87 μM/30 μM=53%. Therefore, only 53% of the 30 μM CF was in hexagonal arrays and the remaining 47% in Koshy's study were non-array CF bound to the vesicles.

A2. Justification of lipid concentration used in this study

In this study, 30 μM His-tagged CF was assembled onto 725 μM total lipid with CheA and CheW. This lipid condition was chosen to have maximum kinase activity for both CF4Q and CF4E, and exhibited the physiological stoichiometry of 6 CF:1 CheA: 2 CheW in the sedimented arrays. Note that crowded conditions must be chosen to induce the kinase-on state of CF4E (Besschetnova et al., 2008). Under our assembly conditions, an average of 27 μM CF sedimented in arrays with CheA and CheW (calculated from 0 and 16 hour time points in Table 3.1). For vesicles extruded through 100 nm membranes, Montefusco et al reported a 59 nm diameter (Montefusco et al., 2006). This predicts the outer leaflet has 51% and the inner leaflet has 49% of the vesicle surface area. Thus we calculate an available surface area of 9.93 nm^2 per CF on the surface of these vesicles:

$$\frac{725\ \mu M\ total\ lipid}{27\ \mu M\ CF} \cdot 0.51\ lipid\ outlerleaflet \cdot \frac{0.725\ nm^2}{lipid} = \frac{9.93\ nm^2}{CF}$$

This is sufficient for 96% of the CF to bind in hexagonal arrays.

$$\frac{9.93\ nm^2}{10.4\ nm^2} = 95.5\%$$

This calculation neglects the area occupied by the CF not in arrays. If we don't neglect this (instead do the calculation as done in section A1 above), the result is that 91% of bound CF is in arrays.

The HDX behavior of the ~10% CF that does not bind to vesicles and the ~10% CF that is bound but not in arrays should be negligible. The unbound CF would fully exchange at 3 min and then have no further influence on the HDX. The bound non-array CF would not exhibit complete HDX in 3 min, based on the results of Koshy et al on samples with

47% bound non-array CF. Thus these two 10% populations would exhibit different HDX, and none of the conclusions of our HDX study are based on a 10% fraction.

A slightly higher lipid concentration [10.4 nm^2/CF * 30 μM CF * (2 lipid/0.725 nm^2 DOPC bilayer surface area) = 860 μM lipid] might have been better in order to incorporate all of the CF into the arrays, but might also have made it difficult to reproducibly crowd the CF4E into the kinase-on state.

BIBLIOGRAPHY

Amin, D. N.; Hazelbauer, G. L. Influence of Membrane Lipid Composition on a Transmembrane Bacterial Chemoreceptor. *J. Biol. Chem.* **2012**, *287* (50), 41697–41705.

Aravind, L.; Ponting, C. P. The Cytoplasmic Helical Linker Domain of Receptor Histidine Kinase and Methyl-Accepting Proteins Is Common to Many Prokaryotic Signalling Proteins. *FEMS Microbiol. Lett.* **1999**, *176* (1), 111–116.

Bartelli, N. L.; Hazelbauer, G. L. Bacterial Chemoreceptor Dynamics: Helical Stability in the Cytoplasmic Domain Varies with Functional Segment and Adaptational Modification. *J. Mol. Biol.* **2016**, *428* (19), 3789–3804.

Besschetnova, T. Y.; Montefusco, D. J.; Asinas, A. E.; Shrout, A. L.; Antommattei, F. M.; Weis, R. M. Receptor Density Balances Signal Stimulation and Attenuation in Membrane-Assembled Complexes of Bacterial Chemotaxis Signaling Proteins. *Proc. Natl. Acad. Sci. U. S. A.* **2008**, *105* (34), 12289–12294.

Briegel, A.; Ding, H. J.; Li, Z.; Werner, J.; Gitai, Z.; Dias, D. P.; Jensen, R. B.; Jensen, G. J. Location and Architecture of the Caulobacter Crescentus Chemoreceptor Array. *Mol. Microbiol.* **2008**, *69* (1), 30–41.

Briegel, A.; Ortega, D. R.; Tocheva, E. I.; Wuichet, K.; Li, Z.; Chen, S.; Muller, A.; Iancu, C. V; Murphy, G. E.; Dobro, M. J.; et al. Universal Architecture of Bacterial Chemoreceptor Arrays. *Proc Natl Acad Sci U S A* **2009**, *106* (40), 17181–17186.

Briegel, A.; Ames, P.; Gumbart, J. C.; Oikonomou, C. M.; Parkinson, J. S.; Jensen, G. J. The Mobility of Two Kinase Domains in the Escherichia Coli Chemoreceptor Array Varies with Signalling State. *Mol. Microbiol.* **2013**, *89* (5), 831–841.

Briegel, A.; Wong, M. L.; Hodges, H. L.; Oikonomou, C. M.; Piasta, K. N.; Harris, M. J.; Fowler, D. J.; Thompson, L. K.; Falke, J. J.; Kiessling, L. L.; et al. New Insights into Bacterial Chemoreceptor Array Structure and Assembly from Electron Cryotomography. *Biochemistry* **2014**, *53* (10), 1575–1585.

Briegel, a.; Li, X.; Bilwes, a. M.; Hughes, K. T.; Jensen, G. J.; Crane, B. R. Bacterial Chemoreceptor Arrays Are Hexagonally Packed Trimers of Receptor Dimers Networked by Rings of Kinase and Coupling Proteins. *Proc. Natl. Acad. Sci.* **2012**, *109* (10), 3766–3771.

Cassidy, C. K.; Himes, B. A.; Alvarez, F. J.; Ma, J.; Zhao, G.; Perilla, J. R.; Schulten, K.; Zhang, P. CryoEM and Computer Simulations Reveal a Novel Kinase Conformational Switch in Bacterial Chemotaxis Signaling Department of Physics and Beckman Institute , University of Illinois at Urbana-Champaign , Urbana , IL 61801 , USA Department of Structural Biolo. **2015**, No. November.

Chervitz, S. a; Falke, J. J. Molecular Mechanism of Transmembrane Signaling by the Aspartate Receptor: A Model. *Proc. Natl. Acad. Sci. U. S. A.* **1996**, *93* (6), 2545–2550.

Chung, K. Y.; Rasmussen, S. G. F.; Liu, T.; Li, S.; Devree, B. T.; Chae, P. S.; Calinski, D.; Kobilka, B. K.; Woods, V. L.; Sunahara, R. K. Conformational Changes in the G Protein Gs Induced by the β 2 Adrenergic Receptor. *Nature* **2011**, *477* (7366), 611–617.

Duc, N. M.; Du, Y.; Thorsen, T. S.; Lee, S. Y.; Zhang, C.; Kato, H.; Kobilka, B. K.; Chung, K. Y. Effective Application of Bicelles for Conformational Analysis of G Protein-Coupled Receptors by Hydrogen/deuterium Exchange Mass Spectrometry. *J. Am. Soc. Mass Spectrom.* **2015**, *26* (5), 808–817.

Falke, J. J.; Hazelbauer, G. L. Transmembrane Signaling in Bacterial Chemoreceptors. *Trends Biochem. Sci.* **2001**, *26* (4), 257–265.

Fowler, D. J.; Weis, R. M.; Thompson, L. K. Kinase-Active Signaling Complexes of Bacterial Chemoreceptors Do Not Contain Proposed Receptor-Receptor Contacts Observed in Crystal Structures. *Biochemistry* **2010**, *49* (7), 1425–1434.

Gegner, J. A.; Dahlquist, F. W. Signal Transduction in Bacteria: CheW Forms a Reversible Complex with the Protein Kinase CheA. *Proc Natl Acad Sci U S A* **1991**, *88* (3), 750–754.

Guttman, M.; Weis, D. D.; Engen, J. R.; Lee, K. K. Analysis of Overlapped and Noisy Hydrogen/Deuterium Exchange Mass Spectra. *J. Am. Soc. Mass Spectrom* **2013**, *24*, 1906–1912.

Haglin, E. R. Assembly and Functional Architechture of Bacterial Chemoreceptor Nanoarrays. ScholarWorks 2018, p 132.

Haglin, E. R.; Yang, W.; Briegel, A.; Thompson, L. K. His-Tag-Mediated Dimerization of Chemoreceptors Leads to Assembly of Functional Nanoarrays. *Biochemistry* **2017**, *56* (44), 5874–5885.

Houde, D.; Berkowitz, S. A.; Engen, J. R. The Utility of Hydrogen/deuterium Exchange Mass Spectrometry in Biopharmaceutical Comparability Studies. *J. Pharm. Sci.* **2011**, *100* (6), 2071–2086.

Kacprzyk-Stokowiec, A.; Kulma, M.; Traczyk, G.; Kwiatkowska, K.; Sobota, A.; Dadlez, M. Crucial Role of PerfringolysinOD1 Domain in Orchestrating Structural Transitions Leading to Membrane-Perforating Pores: A Hydrogen-Deuterium Exchange Study. *J. Biol. Chem.* **2014**, *289* (41), 28738–28752.

Kapust, R. B.; Tözsér, J.; Fox, J. D.; Anderson, D. E.; Cherry, S.; Copeland, T. D.; Waugh, D. S. Tobacco Etch Virus Protease: Mechanism of Autolysis and Rational Design of Stable Mutants with Wild-Type Catalytic Proficiency. *Protein Eng.* **2001**, *14* (12), 993–1000.

Kashefi, M.; Thompson, L. K. Signaling-Related Mobility Changes in Bacterial Chemotaxis Receptors Revealed by Solid-State NMR. *J. Phys. Chem. B* **2017**, *121* (37), 8693–8705.

Kim, K. K.; Yokota, H.; Kim, S. H. Four-Helical-Bundle Structure of the Cytoplasmic Domain of a Serine Chemotaxis Receptor. *Nature* **1999**, *400* (6746), 787–792.

Koshy, S. S.; Li, X.; Eyles, S. J.; Weis, R. M.; Thompson, L. K. Hydrogen Exchange Di Ff Erences between Chemoreceptor Signaling Complexes Localize to Functionally Important Subdomains. *Biochemistry* **2014**, *53* (49), 7755–7764.

Li, G.; Weis, R. M. Covalent Modification Regulates Ligand Binding to Receptor Complexes in the Chemosensory System of Escherichia Coli. *Cell* **2000**, *100* (3), 357–365.

Lukat, G. S.; Lee, B. H.; Mottonen, J. M.; Stock, A. M.; Stock, J. B. Roles of the Highly Conserved Aspartate and Lysine Residues in the Response Regulator of Bacterial Chemotaxis. *J. Biol. Chem.* **1991**, *266* (13), 8348–8354.

Maddock, J. R.; Shapiro, L. Polar Location of the Chemoreceptor Complex in the Escherichia Coli Cell. *Science* **1993**, *259* (5102), 1717–1723.

Marcsisin, S. R.; Engen, J. R. Hydrogen Exchange Mass Spectrometry: What Is It and What Can It Tell Us? *Anal. Bioanal. Chem.* **2010**, *397* (3), 967–972.

Mo, G.; Zhou, H.; Kawamura, T.; Dahlquist, F. W. Solution Structure of a Complex of the Histidine Auto Kinase CheA with Its Substrate CheY. *Biochemistry* **2012**, *51* (18), 3786–3798.

Montefusco, D. J.; Shrout, A. L.; Besschetnova, T. Y.; Weis, R. M. Formation and Activity of Template-Assembled Receptor Signaling Complexes. *Langmuir* **2006**, *23* (6), 3280–3289.

Morgan, C. R.; Hebling, C. M.; Rand, K. D.; Stafford, D. W.; Jorgenson, J. W.; Engen, J. R. Conformational Transitions in the Membrane Scaffold Protein of Phospholipid Bilayer Nanodiscs. *Mol. Cell. Proteomics* **2011**, *10* (9), M111.010876.

Murphy, O. J.; Yi, X.; Weis, R. M.; Thompson, L. K. Hydrogen Exchange Reveals a Stable and Expandable Core within the Aspartate Receptor Cytoplasmic Domain. *J. Biol. Chem.* **2001**, *276* (46), 43262–43269.

Nagle, J. F.; Tristram-Nagle, S. Structure of Lipid Bilayers. *Biochim. Biophys. Acta - Rev. Biomembr.* **2000**, *1469* (3), 159–195.

Ottemann, K. M.; Xiao, W.; Shin, Y.-K.; Koshland, D. E. A Piston Model for Transmembrane Signalling of the Aspartate Receptor. *Science (80-.).* **1999**, *285* (5434), 1751–1754.

Pedetta, A.; Parkinson, J. S.; Studdert, C. A. Signalling-Dependent Interactions between the Kinase-Coupling Protein CheW and Chemoreceptors in Living Cells. *Mol. Microbiol.* **2014**, *93* (6), 1144–1155.

Samanta, D.; Borbat, P. P.; Dzikovski, B.; Freed, J. H.; Crane, B. R. Bacterial Chemoreceptor Dynamics Correlate with Activity State and Are Coupled over Long Distances. *Proc. Natl. Acad. Sci.* **2015**, *2* (10), 2455–2460.

Schneider, C. A.; Rasband, W. S.; Eliceiri, K. W. NIH Image to ImageJ : 25 Years of Image Analysis HISTORICAL Commentary NIH Image to ImageJ : 25 Years of Image Analysis. *Nat. Methods* **2012**, *9* (7), 671–675.

Shrout, A. L.; Montefusco, D. J.; Weis, R. M. Template-Directed Assembly of Receptor Signaling Complexes. *Biochemistry* **2003**, *42* (46), 13379–13385.

Sourjik, V.; Berg, H. C. Receptor Sensitivity in Bacterial Chemotaxis. *Proc. Natl. Acad. Sci. U. S. A.* **2002**, *99* (1), 123–127.

Swain, K. E.; Gonzalez, M. A.; Falke, J. J. Engineered Socket Study of Signaling through a Four-Helix Bundle: Evidence for a Yin-Yang Mechanism in the Kinase Control Module of the Aspartate Receptor. *Biochemistry* **2009**, *48* (39), 9266–9277.

Vu, A.; Wang, X.; Zhou, H.; Dahlquist, F. W. The Receptor-CheW Binding Interface in Bacterial Chemotaxis. *J. Mol. Biol.* **2012**, *415* (4), 759–767.

Wadhams, G. H.; Armitage, J. P. Making Sense of It All: Bacterial Chemotaxis. *Nat. Rev. Mol. Cell Biol.* **2004**, *5* (12), 1024–1037.

Wang, X.; Vu, A.; Lee, K.; Dahlquist, F. W. CheA-Receptor Interaction Sites in Bacterial Chemotaxis. *J. Mol. Biol.* **2012a**, *422* (2), 282–290.

Wang, X.; Wu, C.; Vu, A.; Shea, J. E.; Dahlquist, F. W. Computational and Experimental Analyses Reveal the Essential Roles of Interdomain Linkers in the Biological Function of Chemotaxis Histidine Kinase CheA. *J. Am. Chem. Soc.* **2012b**, *134* (39), 16107–16110.

Weis, D. D.; Wales, T. E.; Engen, J. R.; Hotchko, M.; Eyck, L. F. Ten. FOCUS: HYDROGEN EXCHANGE AND COVALENT MODIFICATION Identification and Characterization of EX1 Kinetics in H/D Exchange Mass Spectrometry by Peak Width Analysis. *J Am Soc Mass Spectrom* **2006**, *17*, 1498–1509.

Xiao, H. U. I.; Hoerner, J. K.; Eyles, S. J.; Dobo, A.; Kaltashov, I. A.; Voigtman, E.; C, A. I. M. E. L. Mapping Protein Energy Landscapes with Amide Hydrogen Exchange and Mass Spectrometry : I . A Generalized Model for a Two-State Protein and Comparison with Experiment. *Protein Sci.* **2005**, *14*, 543–557.

Zhang, P.; Khursigara, C. M.; Hartnell, L. M.; Subramaniam, S. Direct Visualization of Escherichia Coli Chemotaxis Receptor Arrays Using Cryo-Electron Microscopy. *Proc. Natl. Acad. Sci. U. S. A.* **2007**, *104* (10), 3777–3781.

Zhou, Q.; Ames, P.; Parkinson, J. S. Mutational Analyses of HAMP Helices Suggest a Dynamic Bundle Model of Input-Output Signalling M Chemoreceptors. *Mol. Microbiol.* **2009**, *73* (5), 801–814.